JOURNAL OF GEOPHYSICAL RESEARCH, VOL. 113, D08204, doi:10.1029/2007JD009388, 2008

Click Here for Full Article

Characterization of atmospheric aerosols using MFRSR measurements

Mikhail D. Alexandrov,[1,2] Andrew A. Lacis,[3] Barbara E. Carlson,[3] and Brian Cairns[1,2]

Received 13 September 2007; revised 26 November 2007; accepted 7 January 2008; published 22 April 2008.

[1] Measurements by multifilter rotating shadowband radiometers (MFRSRs) constitute a valuable global data set with contributions from hundreds of instruments deployed worldwide. The geographical coverage of MFRSR networks is complementary to that of AERONET and often provides better spatial density of measurement sites, especially in the United States. We describe our recently updated analysis algorithm for MFRSR data that allows partitioning of the spectral aerosol optical depth (AOD) into fine and coarse mode AOD and retrieval of the fine mode effective radius. Our recent sensitivity study demonstrated that for a typical measurement accuracy 0.01 of AOD, the trade-offs between the spectral aerosol extinction and NO_2 absorption in the visible range effectively prevent unambiguous retrieval of NO_2 column from MFRSR data and may also bias aerosol size distribution retrievals. This has prompted us to adopt a new retrieval approach, which utilizes climatological NO_2 (based on SCIAMACHY satellite retrievals) and uses column ozone from TOMS measurements. The performance of this new approach was evaluated using the long-term data set from the Southern Great Plains (SGP) site operated by the U.S. Department of Energy Atmospheric Radiation Measurement (ARM) Program. We present a detailed intercomparison of total, fine, and coarse mode AOD and fine mode effective radius between two MFRSRs located at the SGP's Central Facility and with the correlative AERONET Sun-sky inversion results (Version 2) derived from a collocated CIMEL Sun photometer. The comparison between two MFRSRs demonstrated good consistency of both the measurements and the analysis. Agreement with AERONET inversions is remarkably good, in that differences in AOD components do not exceed the expected measurement accuracy of 0.01, while the retrieved values of fine mode effective radius show no relative bias and only 0.03 μm random error (standard deviation of the differences). We show that if only data with large enough AOD (more than 0.06 at 870 nm) are selected, this error is reduced by a factor of two, becoming about 10% of a typical fine mode effective radius value.

Citation: Alexandrov, M. D., A. A. Lacis, B. E. Carlson, and B. Cairns (2008), Characterization of atmospheric aerosols using MFRSR measurements, *J. Geophys. Res.*, *113*, D08204, doi:10.1029/2007JD009388.

1. Introduction

[2] Ground-based Sun photometry is an important source of information for characterization of atmospheric aerosols, and provides a validation tool for global satellite aerosol retrievals. Sun photometric measurements are performed by various types of instruments often deployed in local, regional, or global networks. Aerosol Robotic Network (AERONET) [cf. *Holben et al.*, 1998] using CIMEL Sun/sky radiometers is probably the best known of them. Another Sun photometer, the multifilter rotating shadowband radiometer (MFRSR), is also widely used for measurements of visible range spectral aerosol optical depth (AOD). (According to the AMS Glossary of Meteorology, optical thickness gives the line integral of extinction along any line of sight (e.g., Sun photometer to the Sun), while optical depth is optical thickness projected onto a vertical path. This definition is consistent with terminology used by the WMO Guide to Meteorological Instruments and Methods of Observation.) MFRSR measurements constitute a valuable global data set with contributions from hundreds of instruments deployed worldwide. The major programs running MFRSR networks in the United States include DOE Atmospheric Radiation Measurement (ARM) Program [*Ackerman and Stokes*, 2003], USDA UV-B Monitoring and Research Program [*Bigelow et al.*, 1998], NOAA Surface Radiation (SURFRAD) Network [*Augustine et al.*, 2005], and NASA Solar Irradiance Research Network (SIRN). Internationally MFRSRs are operated mostly by individual users. However, many stations of the World Climate Research Programme

[1]Department of Applied Physics and Applied Mathematics, Columbia University, New York, New York, USA.
[2]Also at NASA Goddard Institute for Space Studies, New York, New York, USA.
[3]NASA Goddard Institute for Space Studies, New York, New York, USA.

Copyright 2008 by the American Geophysical Union.
0148-0227/08/2007JD009388$09.00

(WCRP) Baseline Surface Radiation Network (BSRN) [*Ohmura et al.*, 1998] and Australian Bureau of Meteorology Solar and Terrestrial Network [*Mitchell and Forgan*, 2003] are equipped with these instruments. Unlike AERONET, which provides advanced data analysis products such as aerosol size distribution parameters and absorption properties [*Dubovik and King*, 2000; *Dubovik et al.*, 2002], MFRSR data for the most part remain underutilized, with spectral AOD and Angstrom exponent being the only significant retrieval products available from the major networks on a regular basis. Besides our previous work, comprehensive retrievals of aerosol properties from MFRSR measurements were attempted only on short-term (1 d to 1 month) data sets [*Kassianov et al.*, 2005, 2007].

[3] For the past several years we have worked to fill this gap by designing, improving, and testing retrieval algorithms for MFRSR data to provide aerosol size distribution parameters [*Alexandrov et al.*, 2002a, 2005]. Unfortunately, the inversion of aerosol size from MFRSR data is complicated by trade-offs between spectral absorption of NO_2 in blue wavelength range and the extinction of small aerosol particles. This problem is not specific to only MFRSRs: AERONET retrievals are also affected by significant NO_2 absorption in 440 nm channel of CIMEL. But, until recently NO_2 was not in the focus of the remote sensing community, thus, measurements (discussed in section 9 in more detail) suitable for validation and improvement of Sun photometric algorithms were rare. While available satellite retrievals of NO_2 columns from GOME [*Burrows et al.*, 1999; *Richter and Burrows*, 2002] and SCIAMACHY [*Bovensmann et al.*, 1999; *Richter et al.*, 2004, 2005] have limited accuracy over populated areas where a significant portion of the NO_2 is located in the boundary layer, more accurate ground-based spectrometric studies were focused mostly on stratospheric NO_2, or, in few cases, on the extreme pollution events [e.g., *Schroeder and Davies*, 1987; *Pujadas et al.*, 2000; *Kambezidis et al.*, 2001], reporting unusually large NO_2 amounts. Recently the situation has been improved with publication of several spectrometric studies [*Petritoli et al.*, 2004; *Heue et al.*, 2005; *Wang et al.*, 2005; *Gianelli et al.*, 2005; *Cede et al.*, 2006] providing a realistic variability range of NO_2 column (0.5–3 DU, with mean under 1 DU) over areas moderately affected by urban or industrial pollutions.

[4] We will show in this paper, that given a wide enough range of realistic aerosol size distributions, the trade-offs between NO_2 absorption and fine mode aerosol extinction effectively prevent unambiguous retrievals of NO_2 column using the sparse spectral sampling typical of Sun photometers. AERONET originally neglected NO_2 in their retrievals, however, in the recently released Version 2 retrieval product, satellite-based NO_2 climatology is used. *Kassianov et al.* [2005, 2007] did not specifically account for NO_2 absorption in their MFRSR retrievals. Our original approach included NO_2 retrievals, but the importance of correctly specifying aerosol size distribution shape was not clearly established. *Alexandrov et al.* [2002a] used a simplified monomodal aerosol size model, which tends to produce large NO_2 columns that are strongly correlated with AOD [*Alexandrov et al.*, 2002b]. In our next study [*Alexandrov et al.*, 2005] a more realistic bimodal aerosol model was adopted. That model was essentially the same as in the present paper, with one important difference: the fine mode effective radius was not allowed to be smaller than 0.2 μm. In retrospect, this cutoff value was too large: while the NO_2 column amounts retrieved with the new aerosol model were smaller by about a factor of two compared with *Alexandrov et al.* [2002b], they still remained too high and too strongly correlated with AOD.

[5] Our experience shows, that since the retrieved NO_2 column values depend on the particular constraints imposed on the family of possible aerosol size distributions, column NO_2 cannot be retrieved from Sun photometric data with typical MFRSR spectral sampling and measurement accuracy. While the admissible range of NO_2 amounts is finite, the errors exceed climatological maximum amounts making such retrievals pointless. Accordingly, we have adopted a new retrieval approach which focuses on aerosol properties while utilizing climatological amounts of NO_2 compiled from recent SCIAMACHY satellite retrievals and ozone from TOMS satellite measurements.

[6] In this paper we describe the new retrieval algorithm and show the results of its application to the MFRSR data set from the U.S. Southern Great Plains (SGP) site run by the DOE Atmospheric Radiation Measurement (ARM) Program. This site includes MFRSR network consisting of 21 instruments located at SGP's Central (CF) and Extended Facilities (EFs) in northern Oklahoma and southern Kansas. In this study we focus on two MFRSRs located at SGP's CF. We present a detailed intercomparison of retrievals of total, fine, and coarse mode AOD, and fine mode effective radius between these two instruments and with the correlative AERONET Sun-sky inversion results (Version 2) derived from a CIMEL Sun photometer collocated with the MFRSRs.

2. MFRSR Measurements

[7] The MFRSR [cf. *Harrison et al.*, 1994] makes precise simultaneous measurements of the solar irradiances at six wavelengths (nominally 415, 500, 615, 673, 870, and 940 nm) at short intervals (20 s for ARM instruments) throughout the day. Time series of direct solar beam extinctions and horizontal diffuse fluxes are derived from these measurements. Besides water vapor at 940 nm, the other gaseous absorbers within the MFRSR channels are NO_2 (at 415, 500, and 615 nm) and O_3 (at 500, 615, and 670 nm). Aerosols and Rayleigh scattering contribute atmospheric extinction in all MFRSR channels (Figure 1).

[8] In this study we will demonstrate the performance of the new retrieval algorithm on the year-long (2000) data set from the two ARM-operated MFRSRs C1 and E13 located at the SGP's Central Facility. We note that this data set was not affected by the recently discovered "bug" in the manufacturer's data processing software, which resulted in application of erroneous nighttime offsets to the direct normal irradiances [cf. *Alexandrov et al.*, 2007].

3. Aerosol Model

[9] In this study we adopt a bimodal gamma distribution for the aerosol size distribution model with the effective variance $v_{\mathrm{eff}} = 0.2$ for both modes. The effective radius r_{eff} of the fine mode is a retrievable parameter (we allow it to be

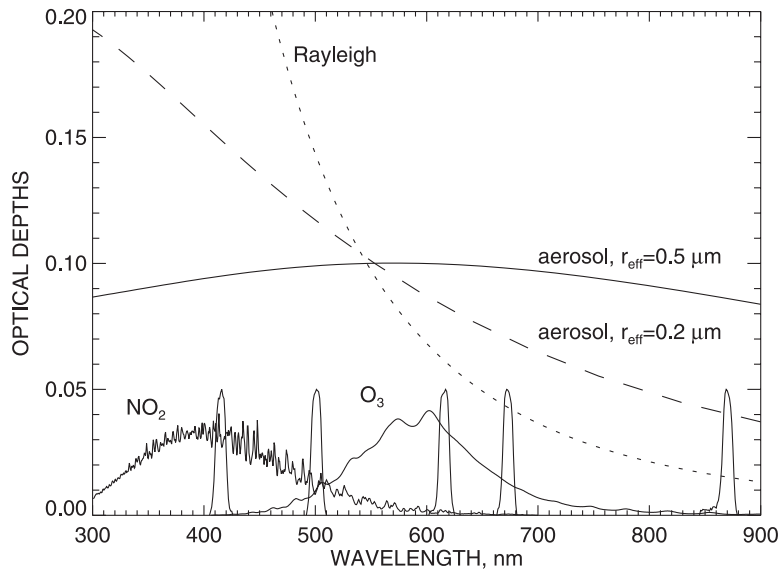

Figure 1. Sample spectral optical depths of atmospheric constituents in 300–900 nm spectral range: Rayleigh (at 1013.25 mbar pressure); aerosols with $r_{\mathrm{eff}} = 0.2$ and 0.5 μm ($v_{\mathrm{eff}} = 0.2$, Gamma distribution) and AOD of 0.1 at 550 nm; NO_2 (2 DU column amount); and ozone (300 DU column amount). The instrument spectral response functions (in arbitrary units) are shown for the first five channels (415–870 nm).

between 0.03 and 0.5 μm in our retrievals), while the coarse mode effective radius is fixed and equal to 1.5 μm (note the difference with the approach of *Kassianov et al.* [2007] who attempt to retrieve the coarse mode particle size). Figure 2 shows the fine and coarse mode spectral AODs (normalized to 870 nm wavelength) computed using Mie theory and corresponding to different particle sizes. The coarse mode AOD in visible spectral range has little sensitivity to the coarse mode particle size, justifying our decision to fix the coarse mode effective radius in our aerosol model.

[10] Knowing r_{eff} together with fine and coarse mode AODs at a single wavelength allows us to restore the AODs for both modes in the whole spectrum. Thus, we can parameterize the spectral bimodal AOD by the following three parameters: τ_a = AOD at 870 nm, fine mode effective radius r_{eff}, and ν_f = fine mode fraction in 870 nm AOD:

$$\nu_f = \frac{\tau_f}{\tau_f + \tau_c} = \frac{N_f Q^f_{\mathrm{ext}} G_f}{N_f Q^f_{\mathrm{ext}} G_f + N_c Q^c_{\mathrm{ext}} G_c}, \tag{1}$$

where τ_f and τ_c are respectively the fine and coarse mode AODs at 870 nm, N_f and N_c are column numbers of fine and coarse mode particles, $Q_{\mathrm{ext}} = Q_{\mathrm{ext}}(\lambda, r_{\mathrm{eff}}, v_{\mathrm{eff}})$ are Mie-derived extinction efficiencies, and $G = G(r_{\mathrm{eff}}, v_{\mathrm{eff}})$ are geometric cross-sectional areas of particles, λ is the wavelength (870 nm in our case). Clearly,

$$\tau_f = \nu_f \cdot \tau_a, \quad \tau_c = \left(1 - \nu_f\right) \cdot \tau_a, \tag{2}$$

$$\tau_a = \tau_f + \tau_c. \tag{3}$$

[11] While our three parameters are functionally independent and, therefore, suitable for retrieval parameterization, they may be in fact physically correlated. For example, an increase of r_{eff} due to, e.g., hygroscopic growth would lead to increase in both τ_a and ν_f. The variables physically independent of particle size (if we do not consider processes like coagulation) are the total number of particles and the particle number fraction

$$\hat{\nu}_f = \frac{N_f}{N_f + N_c}. \tag{4}$$

$\hat{\nu}_f$ is also a parameter of the normalized total aerosol size distribution:

$$n(r) = \hat{\nu}_f n_f(r) + \left(1 - \hat{\nu}_f\right) n_c(r), \tag{5}$$

where $n_f(r)$ and $n_c(r)$ are (normalized) size distribution functions for respective fine and coarse mode aerosol. The relationship between ν_f and $\hat{\nu}_f$ can be written in the following equivalent forms:

$$\nu_f = \frac{\hat{\nu}_f Q^f_{\mathrm{ext}} G_f}{\hat{\nu}_f Q^f_{\mathrm{ext}} G_f + \left(1 - \hat{\nu}_f\right) Q^c_{\mathrm{ext}} G_c}, \tag{6}$$

$$\left(1 - \frac{1}{\hat{\nu}_f}\right)\left(1 - \frac{1}{\nu_f}\right)^{-1} = \frac{Q^f_{\mathrm{ext}} G_f}{Q^c_{\mathrm{ext}} G_c}, \tag{7}$$

$$\hat{\nu}_f = \left[1 - \left(1 - \frac{1}{\nu_f}\right)\frac{Q^f_{\mathrm{ext}} G_f}{Q^c_{\mathrm{ext}} G_c}\right]^{-1}. \tag{8}$$

[12] For gamma distribution

$$G(r_{\mathrm{eff}}, v_{\mathrm{eff}}) = \pi(1 - v_{\mathrm{eff}})(1 - 2v_{\mathrm{eff}}) r^2_{\mathrm{eff}}. \tag{9}$$

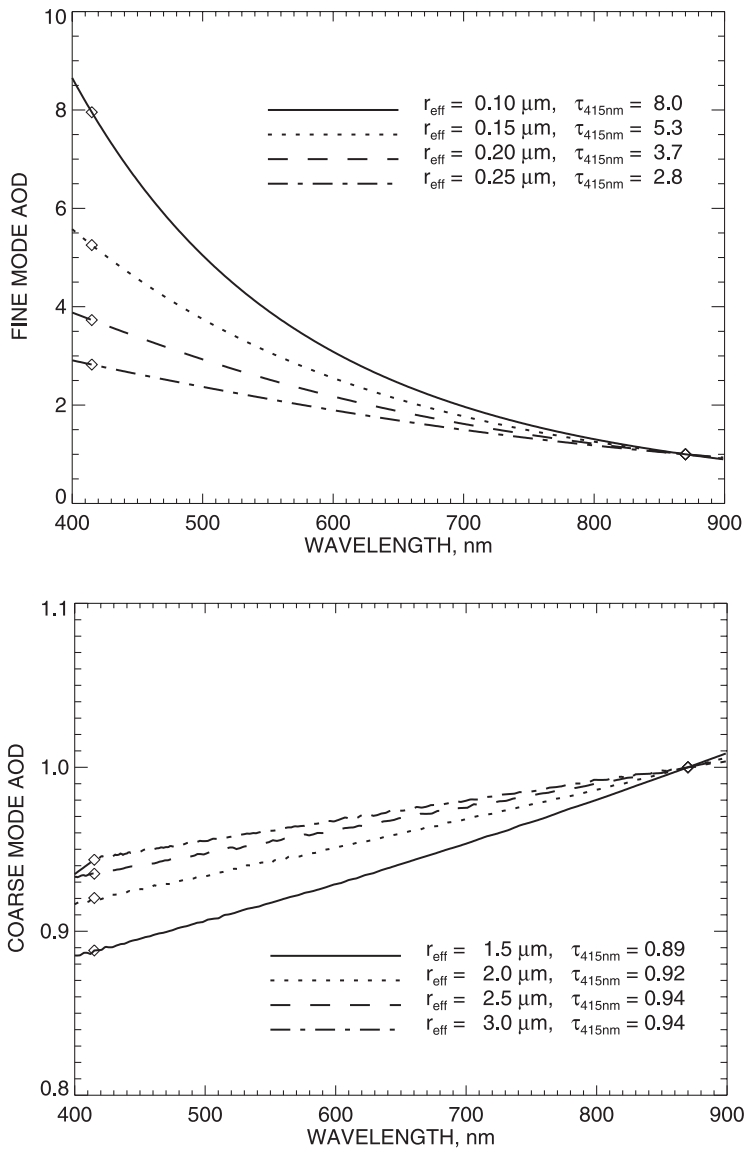

Figure 2. Spectral AOD (normalized to 870 nm wavelength) computed using Mie theory for (top) fine and (bottom) coarse aerosol modes with various effective radii. The aerosol particle size distributions in both cases are modeled by gamma distribution with effective variance 0.2.

[13] Note, that in our parameterization both aerosol modes have the same v_{eff}, which allows cancellation of v_{eff} from equation (8).

[14] We should note, that retrievals from MFRSR data cannot constrain the coarse mode aerosol, and, therefore, are not sufficient for conclusive reconstruction of the total aerosol size distribution shape (5). This is of concern for both $n_c(r)$ and $\hat{v}_f$, which depend on the coarse mode size mainly through G_c. This means, that different size distribution functions can result in very close spectral AODs in the visible range. Thus, the function (5) computed with assumed coarse mode parameters may be quite different from, e.g., AERONET's almucantar size distribution retrievals, even if the fine mode r_{eff} are close.

4. Sensitivity of Aerosol Size Retrievals to Measurement and Model Uncertainties

4.1. Sensitivity to Uncertainties in AOD

[15] The main source of uncertainties in optical depth (OD) measurements by a Sun photometer is the instrument's calibration. This limits the accuracy of AOD derived from AERONET's CIMEL tracking Sun photometer data to ±0.01 for wavelengths longer than 440 nm, and ±0.02 for shorter wavelengths [*Holben et al.*, 1998]. Reported calibration accuracy of MFRSRs, achievable through a long-term Langley analysis, is essentially the same: 0.01 in optical depth [*Michalsky et al.*, 2001]. Shadowband instruments also have some specific accuracy issues in addition to calibration uncertainties. These problems involve instrument tilt and accuracy of angular response determination. *Alexandrov et al.* [2007] present a comprehensive review of measurement and data processing artifacts and their influ-

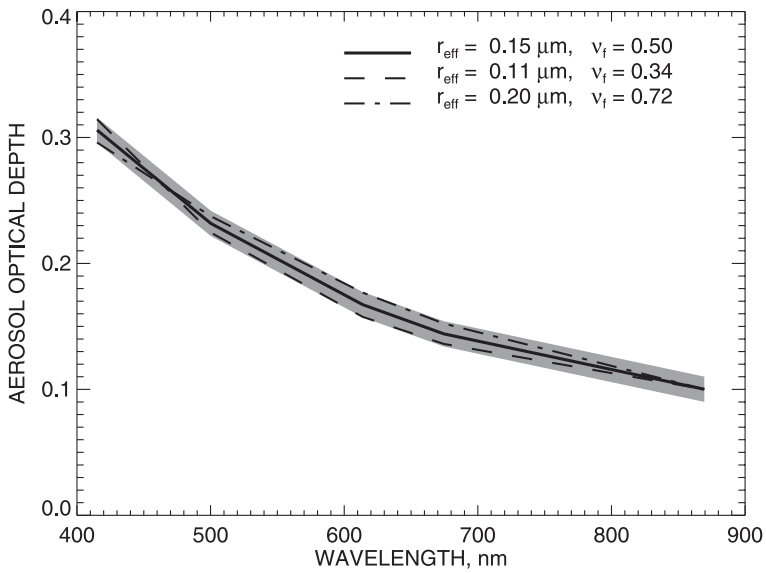

Figure 3. The model spectral AOD curves derived using Mie theory for bimodal gamma aerosol size distribution with fine mode $r_{\mathrm{eff}} = 0.15\mu$m, coarse mode $r_{\mathrm{eff}} = 1.5\mu$m, and fine mode fraction in 870 nm AOD of 0.5. The plot shows MFRSR 415–870 nm spectral range. The two competitive aerosol models fitting within ± 0.01 error margin (grey area) are shown by dashed and dash-dotted lines.

ence on optical depth determination. This study, however, indicates that the MFRSR-specific errors rarely exceed the calibration accuracy of 0.01. Thus the general error propagation analysis presented below is applicable to these uncertainties as well. We should note only that while uncertainties in MFRSR angular response do not have a specific spectral signature, instrument tilts create a wavelength-independent error in optical depth, thus, affecting mainly the coarse mode AOD.

[16] The uncertainty in AOD measurements clearly impacts aerosol size retrievals, since spectral AODs corresponding to different aerosol models may be indistinguishable within the measurement accuracy. To assess the magnitude of this problem, we take a test model spectral AOD $\tau_0(\lambda)$ corresponding to $\tau_a = 0.1$, $\nu_f = 0.50$, and $r_{\mathrm{eff}} = 0.15$ μm and fit it with "retrieved" AODs $\tau(\lambda)$ corresponding to different aerosol models at MFRSR channel wavelengths. For computational simplicity we assume, that AOD at 870 nm is known precisely ($\tau_a = 0.1$), thus, we have only r_{eff} and ν_f to vary. The results are shown in Figure 3. The "retrieved" AODs with the largest and the smallest possible fine mode size are plotted for comparison: $r_{\mathrm{eff}} = 0.11$ μm, $\nu_f = 0.34$; $r_{\mathrm{eff}} = 0.20$ μm, $\nu_f = 0.72$.

[17] A more general picture of sensitivity of MFRSR retrievals of r_{eff} and ν_f to an error of 0.01 in measured AOD is shown in Figure 4. In Figure 4 we present retrieval sensitivity results for 9 test models. The plots from bottom to top correspond to test models with $r_{\mathrm{eff}} = 0.1, 0.15, 0.25$ μm respectively, while each plot shows data for three test aerosol models with fine mode fractions at 870 nm of 0.1, 0.5, and 0.9, each depicted by a bullet in (ν_f, r_{eff}) plane. For each of the test models the interiors of the corresponding black curves (labeled "0 DU") depict the sets of "retrieved" (ν_f, r_{eff}) points corresponding to the models with spectral AODs $\tau(\lambda)$ closer to the test model $\tau_0(\lambda)$ than the measurement accuracy $\varepsilon = 0.01$, i.e.,

$$\| \tau(\lambda) - \tau_0(\lambda) \| = \max_{\lambda_i} |\tau(\lambda_i) - \tau_0(\lambda_i)| < \varepsilon. \qquad (10)$$

Here λ_i, $i = 1, \ldots, 4$, are MFRSR channel wavelengths.

[18] Comparing Figure 4 (top) and Figure 4 (bottom) we see that uncertainties of the retrievals of r_{eff} and ν_f increase with fine mode particle size of the test model. For example, at test model $\nu_f = 0.5$ the retrieval accuracy for fine mode particles with $r_{\mathrm{eff}} = 0.1$ μm is around ±0.02 μm in size and ±0.1 in fine mode fraction, while for 0.25 μm particles these numbers are much larger (respectively ±0.1 μm and ±0.3). This relationship is caused in part by a similarity of spectral extinction by coarse mode and larger fine mode aerosol particles, which makes it difficult to separate between them

Figure 4. Sensitivity of MFRSR retrievals of fine mode effective radius, fine mode fraction in 870 nm AOD, and NO_2 column amount to an error of 0.01 in measured optical depth for 9 test models. Shown are test models with (top) $r_{\mathrm{eff}} = 0.1$ μm, (middle) $r_{\mathrm{eff}} = 0.15$ μm, and (bottom) $r_{\mathrm{eff}} = 0.2$ μm. Each plot shows data for three test models with fine mode fractions at 870 nm of 0.1, 0.5, and 0.9 (each depicted by a bullet). NO_2 amount in test models is zero. AOD at 870 nm is assumed to be known precisely and equal to 0.1. For each of the test models the interiors of the corresponding level curves (labeled with NO_2 amounts assumed in the retrievals) depict the sets of "retrieved" (ν_f, r_{eff}) points corresponding to the "aerosol + NO_2" models with spectral ODs closer than the measurement accuracy to that of the test model.

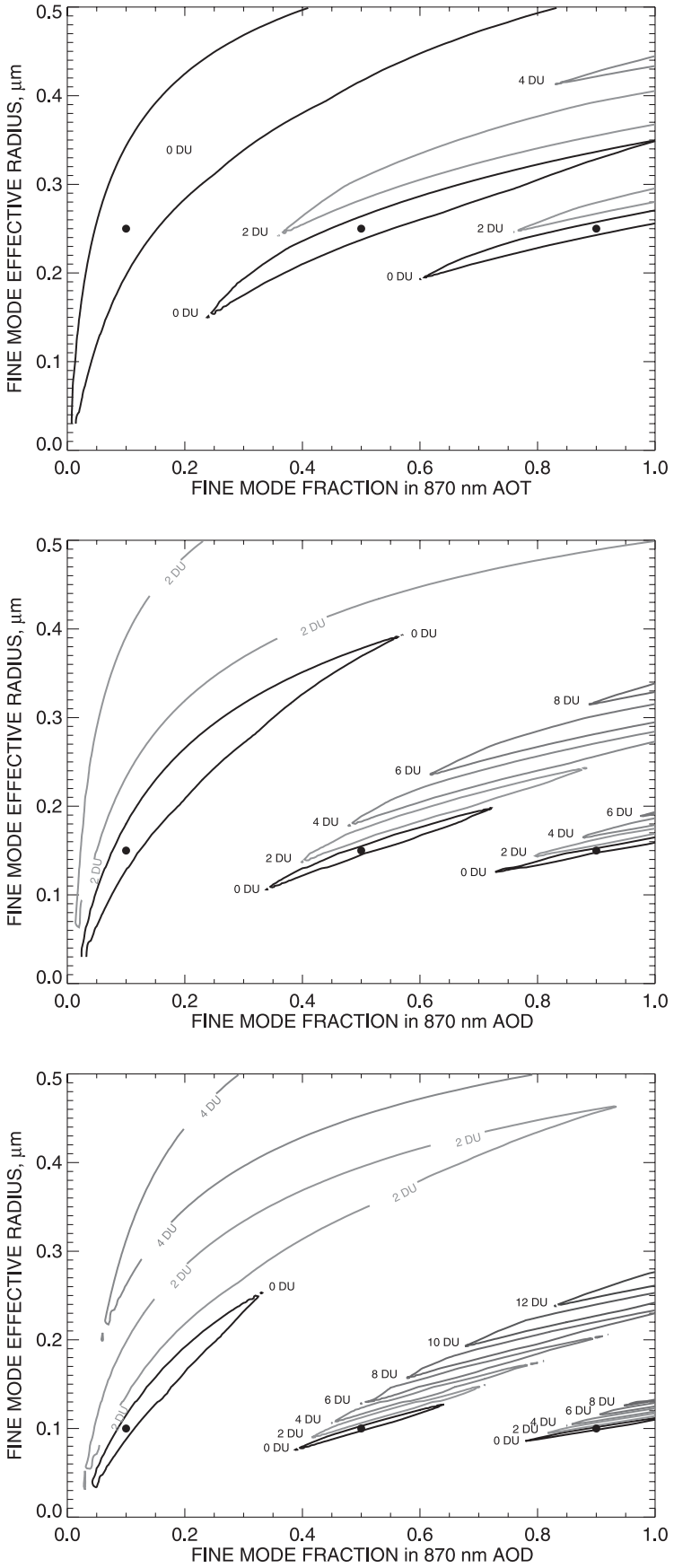
FINE MODE EFFECTIVE RADIUS, µm
FINE MODE FRACTION in 870 nm AOT
0 DU
2 DU
4 DU
FINE MODE EFFECTIVE RADIUS, µm
FINE MODE FRACTION in 870 nm AOD
0 DU
2 DU
4 DU
6 DU
8 DU
FINE MODE EFFECTIVE RADIUS, µm
FINE MODE FRACTION in 870 nm AOD
0 DU
2 DU
4 DU
6 DU
8 DU
10 DU
12 DU

Figure 4

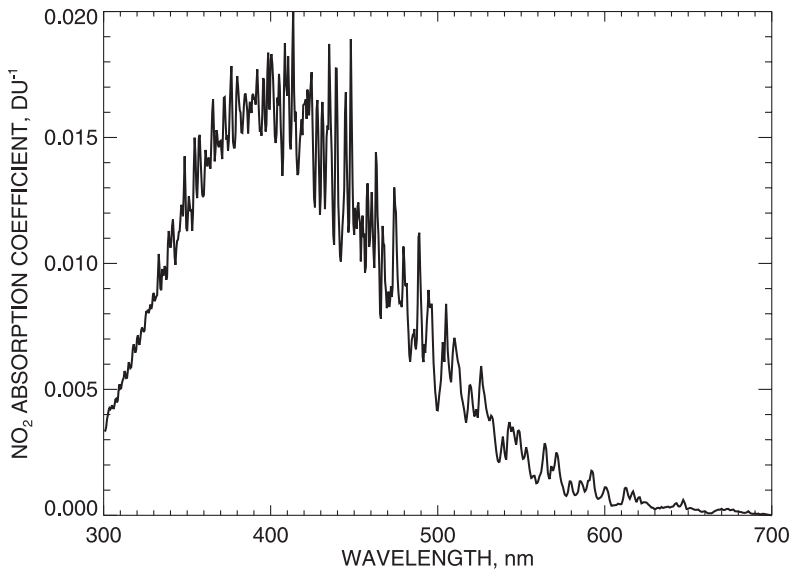

Figure 5. Spectral absorption coefficient of NO_2 in 300–700 nm region. Product of this coefficient and columnar amount of NO_2 in DU is the spectral optical depth due to NO_2 absorption.

with available measurement accuracy. It is also evident from Figure 4 that for each test model fine mode r_{eff} the retrieval uncertainties increase with decrease of fine mode fraction, especially at smaller ν_f. Such loss of accuracy is expected when magnitude of fine mode AOD become comparable with the measurement accuracy. While fine mode AOD in other MFRSR channels is larger than at 870 nm and varies with r_{eff}, we can use AOD at 870 nm to make a conservative estimate of the critical value of ν_f

$$\nu_f^{cr} = \frac{\varepsilon}{\tau(870\mathrm{nm})}, \tag{11}$$

below which, sensitivity of a spectral retrieval algorithm is effectively lost for practical applications. In our test models we assume AOD at 870 nm to be 0.1 and measurement accuracy of 0.01, thus $\nu_f^{cr} = 0.1$. The relation (11) indicates that the accuracy of retrievals will decrease with total AOD (in the extreme case of $\tau \leq \varepsilon$ no reliable retrievals are possible). We will encounter similar relation between retrieval accuracy and AOD later in the paper when we compare retrievals from different instruments. The actual magnitude of loss of the retrieval accuracy at $\nu_f = \nu_f^{cr}$ depends on the fine mode r_{eff} value, as seen in Figure 4 (first model in each plot). It is the worst at large r_{eff}, when fine mode AOD may be comparable with ε in most of MFRSR spectral channels (see Figure 2, top), and the above mentioned similarity between fine and coarse mode spectral AODs starts to play role. However, we see from Figure 4 (bottom) that even at $r_{\mathrm{eff}} = 0.1$ μm the error in retrieved r_{eff} for test model $\nu_f = 0.1$ is between 0.05 and 0.1 μm, which makes the retrieval effectively useless.

4.2. Sensitivity to NO_2 Column Amounts

[19] The uncertainties in retrievals of aerosol size distribution parameters significantly increase if we assume the presence of an undetermined NO_2 column amount. Spectral absorption of NO_2 (Figure 5) in visible and near UV range has significant trade-offs with extinction of small aerosol particles. This can be seen qualitatively from Figure 1. To quantify the extent of these trade-offs we perform a simulation similar to that described above. We take the same test spectral AOD $\tau_0(\lambda)$ ($\tau_a = 0.1$, $\nu_f = 0.50$, $r_{\mathrm{eff}} = 0.15$ μm and zero NO_2 column) and fit it with spectral optical depths corresponding to different "aerosol + NO_2" models within the measurement accuracy. Figure 6 shows that the models fitting the original spectral AOD within 0.01 accuracy may include up to 8 DU of NO_2, while improving the measurement accuracy to 0.005 reduces this amount only to 6 DU. The grey lines in Figure 4 present an overview of this sensitivity, with the interiors of these lines representing sets of models that include both aerosol and NO_2 (1–12 DU) contributions with spectral OD fits to the corresponding NO_2-free test model (depicted by bullet) to within 0.01 accuracy. We see, that increasing the NO_2 amount necessary for the fit is associated with a simultaneous increase in both fine mode r_{eff} and ν_f. This is explained by the fine mode AOD (Figure 2, top) in shortwave spectral region (within the NO_2 absorption band, Figure 5) being interpreted as AOD of larger fine particles (with smaller spectral slope) coupled with absorption optical depth of NO_2. Outside the NO_2 absorption band the resulting decrease in spectral slope of total AOD has to be compensated by increase in fine mode fraction.

[20] We see from Figure 4, that the smaller the fine mode particles, the larger is the NO_2 amount for which they can be "traded." The largest NO_2 amounts correspond to monomodal size distributions ($\nu_f = 1$), raising concern about retrievals using relatively narrow class of aerosol size distributions. Restrictions imposed on aerosol size distributions may artificially reduce the uncertainty of both aerosol parameters and NO_2 column values, while actually moving the solution into unrealistic territory. We tested such possibilities in our previous work, where either a monomodal size distribution ($\nu_f = 1$) was assumed [*Alexandrov et al.*, 2002a, 2002b], or fine mode effective radius range was restricted to $r_{\mathrm{eff}} \geq 0.2$ μm [*Alexandrov et al.*, 2005]. As we can see from Figure 4, both these restrictions lead to

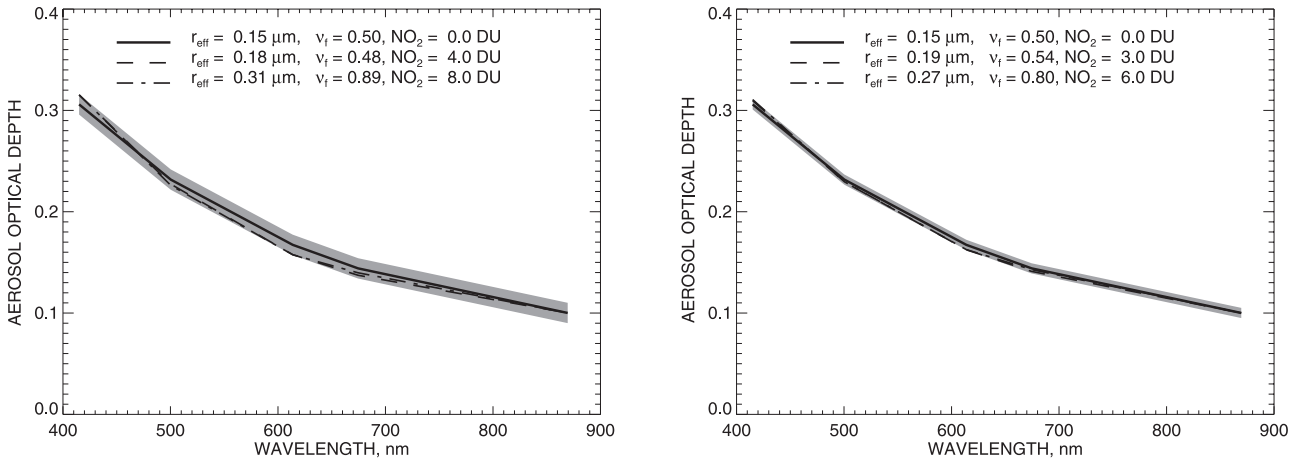

Figure 6. Same as in Figure 3 but with the addition of some preassumed spectral NO_2 absorption to the fit AOD curves. The amount of the added NO_2 is 3 to 8 DU. The assumed measurement accuracy is (left) 0.01 and (right) 0.005.

overestimation of both fine r_{eff} and NO_2 columns. This can also lead to strong correlation between NO_2 columns and AOD, which was also observed in our monomodal retrieval data sets [*Alexandrov et al.*, 2002b]. Similar results were obtained from comparison between monomodal Sun photometric and DOAS retrievals of NO_2 column from the rotating shadowband spectroradiometer (RSS) reported by *Gianelli et al.* [2005].

[21] It can be seen from Figures 1 and 5 that NO_2 spectral absorption decreases with decreasing wavelength in the UV region, while spectral AOD (for, e.g., r_{eff} = 0.2 μm) continues to grow. This suggests that addition of UV channels (like CIMEL's 340 and 380 nm) may help to better constrain aerosol fine mode size and NO_2 amounts. Nevertheless, even the improved accuracy of NO_2 column retrievals in those cases appeared to be no better than ±1 DU. Thus, these retrievals are not able to provide information on NO_2 variability within the realistic range 0–2 DU [*Cede et al.*, 2006; *Gianelli et al.*, 2005; *Richter et al.*, 2005; *Richter and Burrows*, 2002].

[22] Tests show that the spectral optical depth of typical MFRSR measurements can be interpreted by a variety of aerosol models consistent with different NO_2 column amounts ranging from zero to as large as 12 DU. This means, that the spectral range and resolution of MFRSR measurements is not sufficient even to constrain the NO_2 column amount. Thus, it is more effective to take NO_2 values from external sources, i.e., correlative differential absorption measurements (e.g., Brewer spectrometer, RSS), or satellite-based climatology (GOME, SCIAMACHY).

5. Retrieval Algorithm

[23] The retrieval algorithm described in this paper has certain similarities with its previous version [*Alexandrov et al.*, 2005]. The MFRSR data are cloud screened according to [*Alexandrov et al.*, 2004] and Rayleigh optical depth [*Hansen and Travis*, 1974] is subtracted prior to the further analysis. In the current version we do not attempt to retrieve NO_2 column amounts because of the reasons described in section 4.2. Instead we use climatological values compiled from recent SCIAMACHY measurements (overpass data for SGP site have been kindly provided by A. Richter). If no overpass data are available, NO_2 climatology can be obtained from grided monthly mean tropospheric NO_2 SCIAMACHY product [*Richter et al.*, 2005] combined with stratospheric zonal means compiled from GOME total NO_2 climatology [*Richter and Burrows*, 2002] over oceans (where NO_2 is predominantly stratospheric). Both data sets are available at http://www.iup.uni-bremen.de/doas/. These climatological estimates of total NO_2 column amounts do not need to be very precise, since satellite measurements over SGP show almost no values exceeding 0.5 DU, which corresponds to about 0.008 in 415 nm optical depth, and even smaller in other MFRSR channels. Estimation of ozone column amounts from MFRSR data is generally possible [*Michalsky et al.*, 1995; *Taha and Box*, 1999; *Alexandrov et al.*, 2002a, 2002b, 2005], and there are no significant trade-offs between ozone and aerosol parameters. However, the accuracy of these estimates is no better, than that of widely available TOMS and GOME satellite measurements in UV. Indeed, the difference in optical depth caused by an extra 50 DU of ozone at its absorption maximum in the 615 nm MFRSR channel is only 0.005, which is smaller than the usual MFRSR optical depth measurement accuracy. For this reason we have decided to use daily TOMS ozone values instead of deriving ozone columns from the data. Thus, the remaining parameters to be retrieved are primarily fine and coarse mode spectral AOD, and fine mode effective radius. In addition, precipitable water vapor (WV) column is being derived from 940 nm optical depth, and diffuse flux measurements can be used for determination of aerosol spectral single scattering albedo (SSA) [cf. *Kassianov et al.*, 2005, 2007]. These retrievals will be described in separate studies.

5.1. Instrument Calibration From the Data

[24] Laboratory calibrations of MFRSRs (and other Sun photometers) have been shown to lack accuracy [*Michalsky et al.*, 2001; *Kiedron et al.*, 1999; *Schmid et al.*, 1998], and may be unavailable in some cases because of lack of adequate facilities and/or cost. Lab calibration also requires

knowledge of the extraterrestrial spectral irradiance, determination of which has its own uncertainties [*Harrison et al.*, 2003; *Schmid et al.*, 1998]. This emphasizes the need for developing a methodology to allow determination of the instrument's calibrations from observational data. The oldest and still the most widely used calibration method is Langley regression, which requires the optical depth to be constant during the morning or afternoon periods for air mass ranging from 2 to 5. In typical conditions (e.g., continental United States) this is hard to achieve since AOD is quite variable. One way to deal with this variability is by averaging or fitting a smooth curve to the instantaneous daily calibration time series. Some data filtering before the fitting is recommended [*Michalsky et al.*, 2001; *Forgan*, 1988, 1994]. However, this procedure has to be adjusted to keep balance between quality of the regressions selected for averaging and their representativity of the whole calibration history (especially if availability of days suitable for calibration depends on season or other conditions).

[25] Another way of improving calibration from data is by using additional measurements to reduce AOD variability in each individual regression. We use the following two methods. In the first ("direct/diffuse") method [*Alexandrov et al.*, 2002a] we derive an AOD estimate from the calibration-independent ratio of direct normal and diffuse horizontal MFRSR measurements and subtract it from directly measured AOD. The regression on the difference is significantly better than the corresponding Langley plot. However, inversion of AOD from the direct/diffuse ratio requires assumptions of model parameters (aerosol size, SSA, and surface albedo). Uncertainties in these assumptions translates into uncertainties of the derived calibration coefficients. Another variability reduction approach is to have one spectral channel (we take 870 nm) calibrated by other means (e.g., Langley or, as in our approach, direct/diffuse method), then the AOD from this channel can be translated to other channels using relative temporal stability (better than AOD) of aerosol spectral extinction (dependent on the aerosol size distribution and refractive index) [*Forgan*, 1994; *Alexandrov et al.*, 2002a, 2005]. To demonstrate this technique, we assume that we know the 870 nm AOD time series τ_a, and that we have an uncalibrated estimate

$$\tilde{\tau} = q \cdot \tau_a + c\mu \tag{12}$$

of AOD in some other channel with wavelength λ. Here

$$q = \frac{Q_{\text{ext}}(\lambda)}{Q_{\text{ext}}(870\ \text{nm})} \tag{13}$$

is the extinction efficiency factor normalized to 870 nm, μ is the inverse of the air mass (essentially equal to the cosine of the solar zenith angle for small to moderate values of the latter), and c is the calibration coefficient which is equal to zero in the absence of calibration errors. Dividing (12) by μ, we obtain the equation

$$\frac{\tilde{\tau}}{\mu} = q\frac{\tau_a}{\mu} + c, \tag{14}$$

from which c and mean q can be found though a regression in the known parameter τ_a/μ, provided that q is not highly variable.

[26] An advantage of calibration translation method compared to independent channel calibration is its better coherency of the resulting spectral AOD. While possible calibration errors in the 870 nm channel may be translated into other channels with this algorithm, the spectral dependence of AOD (critical for characterization of aerosol size distribution) is preserved, unlike, e.g., in the case when one channel has a calibration error and the others do not. We note, that the described variability reduction techniques are not perfect, thus long-term smoothing of instantaneous calibration time series appears to be necessary. After some initial filtering we use a robust smoothing technique similar to that described by *Cleveland* [1979] and applied by *Michalsky et al.* [2001] to time series of Langley calibrations. Linear interpolation is used for longer periods without days suitable for calibration.

5.2. Derivation of Aerosol Parameters

[27] After all instrument channels are calibrated and spectral AOD is determined, the values of fine mode r_{eff} and fraction in 870 nm AOD ν_f are determined by least square fit. We also suggest a simple analytical procedure, which is almost as accurate as the direct fit, while is significantly faster computationally and, therefore, preferable for test runs. The 870 nm AOD τ_a can be represented as a sum of fine and coarse mode contributions (3):

$$\tau_a = \tau_{870\text{nm}} = \tau_f + \tau_c, \tag{15}$$

while AOD at any other wavelength λ can be written as

$$\tau(\lambda) = q_f(r_{\text{eff}}, \lambda)\ \tau_f + q_c(\lambda)\ \tau_c, \tag{16}$$

where q_f and q_c are respectively fine and coarse mode extinction efficiencies normalized to unity at 870 nm channel (their plots versus wavelength coincide with the plots in Figure 2). Note, that q_c in our model is a predetermined function of wavelength and does not depend on parameters to be retrieved. Using (2) we obtain

$$\frac{\tau}{\tau_a} = \nu_f q_f(r_{\text{eff}}) + \left(1 - \nu_f\right) q_c, \tag{17}$$

or equivalently

$$\frac{\tau}{\tau_a} - q_c = \nu_f\left(q_f(r_{\text{eff}}) - q_c\right). \tag{18}$$

[28] Now, we see, that taking the ratio of such combinations for two different MFRSR channels we can eliminate ν_f and obtain an equation on r_{eff} alone:

$$\frac{(\tau_{415\text{nm}}/\tau_a) - q_c^{(415\text{nm})}}{(\tau_{670\text{nm}}/\tau_a) - q_c^{(670\text{nm})}} = \frac{q_f^{(415\text{nm})}(r_{\text{eff}}) - q_c^{(415\text{nm})}}{q_f^{(670\text{nm})}(r_{\text{eff}}) - q_c^{(670\text{nm})}}. \tag{19}$$

[29] The pair of 415 and 670 nm channels was selected for the largest spectral difference. The left hand side of (19) contains the measured values of $\tau_{415\text{nm}}$, $\tau_{670\text{nm}}$ and $\tau_a = \tau_{870\text{nm}}$, while the right hand side including $q_f(r_{\text{eff}})$ can be

computed using Mie theory and tabulated as function of r_{eff}. After r_{eff} is inverted from (19), ν_f is derived form (18) for any channel (e.g., 415 nm), and spectral fine and coarse mode AODs are computed. Comparison with the results of direct least square fit retrievals shows that, the direct fit produces a more even distribution of residuals between channels, while in the analytical method they are largely concentrated in the "unused" 500 and 615 nm channels. Nevertheless, the values of these residuals are still less than 0.01 (standard deviation less than 0.005), and the differences in residuals between the two methods are around 0.002, i.e., insignificant compared to MFRSR measurement accuracy. There are no noticeable differences in retrieved spectral AOD and r_{eff} between the two approaches.

6. Retrievals From SGP Central Facility MFRSRs

[30] The described retrieval method was applied to MFRSR data for the whole year 2000 from the two MFRSRs collocated at the SGP's Central Facility: C1 and E13. The retrievals from the two instruments were made independently and then compared for a measurement/retrieval consistency check and objective accuracy estimate. Taking into account the high frequency (every 20 s) of MFRSR measurements, it appears impractical to compare the retrievals from individual measurements (point by point). Instead we compared daily mean values. The MFRSR record during the year 2000 provides 269 daily averages to compare. The time series of total, fine, and coarse mode AODs are shown in Figure 7 for the 500 nm wavelength. All three plots show summer maxima (better pronounced in fine mode AOD). The differences between the two instruments are barely discernable.

[31] Figure 8 presents a more detailed AOD scatterplot comparison between C1 and E13 instruments. The plots of total, fine and coarse mode AODs in the first five MFRSR channels are shown. We see that the mean differences in total and fine mode AOD are always below the acceptable calibration accuracy and decrease with wavelength from 0.01 at 415 nm to 0.003 at 870 nm reflecting the fact that shortwave measurements are generally less accurate [cf. *Holben et al.*, 1998] because of smaller signal from the Sun and larger optical depths. The same wavelength dependence is exhibited by the random error (standard deviation of the differences in AOD), which is 0.013 at 415 nm and decreases to 0.005 at 870 nm. The relative bias between the coarse mode AODs from the two MFRSR data sets is practically zero (10^{-4}), while the random error of 0.006–0.007 only weakly depends on the channel wavelength.

[32] Similar intercomparison between the fine mode r_{eff} as well as 415–870 nm Angstrom exponents are presented in Figure 9. As seen from Figure 9 (top), and especially Figure 9 (bottom), agreement between the two instruments appears to be conditional on AOD magnitude. The differences appear to be bounded by values proportional to inverse AOD (the dashed curves in the plots correspond to $\pm 0.003/\tau(870\ \mathrm{nm})$ for r_{eff} and $\pm 0.02/\tau(870\ \mathrm{nm})$ for Angstrom exponent). In the case of Angstrom exponent this relation can be easily derived analytically. It works also for more detailed aerosol size characteristics such as fine mode r_{eff} and fine mode fraction in AOD (cf. *Schuster et al.* [2006] for detailed study of the relationship between Angstrom exponent and bimodal aerosol size distribution parameters). In section 4.1 we also presented a qualitative picture of relationship between AOD value and accuracy of fine mode r_{eff} and ν_f retrievals. While there is no particular critical value of AOD in Figure 9 (bottom), we take $\tau(870\ \mathrm{nm}) = 0.06$ (shown by vertical dash-dotted lines in the plots) to be a reasonable threshold value separating the more reliable retrievals from those less reliable.

[33] It is seen from Figure 9 (top) that, while the mean differences between the two data sets are already very close to zero, restriction to the cases with $\tau(870\ \mathrm{nm}) > 0.06$ notably reduces the standard deviations of these differences (from 0.032 μm to 0.023 μm in fine mode r_{eff}, and from 0.09 to 0.07 in Angstrom exponent). The effect of this restriction can be seen also from the time series of fine mode r_{eff} values shown in Figure 10. Figure 10 (top) presents all available data points, while in Figure 10 (middle) only the data points with $\tau(870\ \mathrm{nm}) > 0.06$ are shown. The latter plot shows less variability in r_{eff} values and better agreement between the two MFRSRs. Both plots show weak seasonal dependence of r_{eff} with slight increase in winter. Multiyear data analysis is needed to see if this behavior is systematic, especially given generally lower AOD in winter (Figure 10, bottom), which may create a sampling bias if the above mentioned restriction is applied. Visual investigation of the data subsets showing the largest discrepancy between C1 and E13 retrievals suggests the following possible causes of the disagreement: (1) the clear sky interval is too short and may in fact be cloudy, thus not suitable for aerosol retrievals; (2) calibrational difference in total AOD between the instruments; (3) small alignment problem (e.g., E13 in the beginning of April 2000); and (4) small AOD, which, as was mentioned above, is associated with more random errors in aerosol size retrievals.

7. Comparisons With AERONET's Sun-Sky Inversions

[34] We have compared our retrievals of total, fine, and coarse mode AODs, and fine mode effective radius with those obtained from AERONET Sun-sky inversion retrievals according to *Dubovik and King* [2000]. These retrievals use sky radiances measured during an almucantar scan together with spectral AOD derived from direct-Sun measurement accomplishing each almucantar sequence [cf. *Holben et al.*, 1998]. The AERONET data were from the CIMEL Sun photometer labeled "Cart Site" on the AERONET web site, which is collocated with the two SGP's Central Facility MFRSRs (C1 and E13). On a clear day, up to 4 AERONET almucantar scan retrievals are available. These retrievals are based on the analysis of both spectral and angular dependencies of the scattered radiation. The advantage of including sky radiation measurements in the analysis is primarily

Figure 7. Daily mean total, fine, and coarse mode AODs in 500 nm channel retrieved from the two SGP's Central Facility MFRSRs (C1 and E13) for the year 2000 (only data points for consecutive days are connected in these plots).

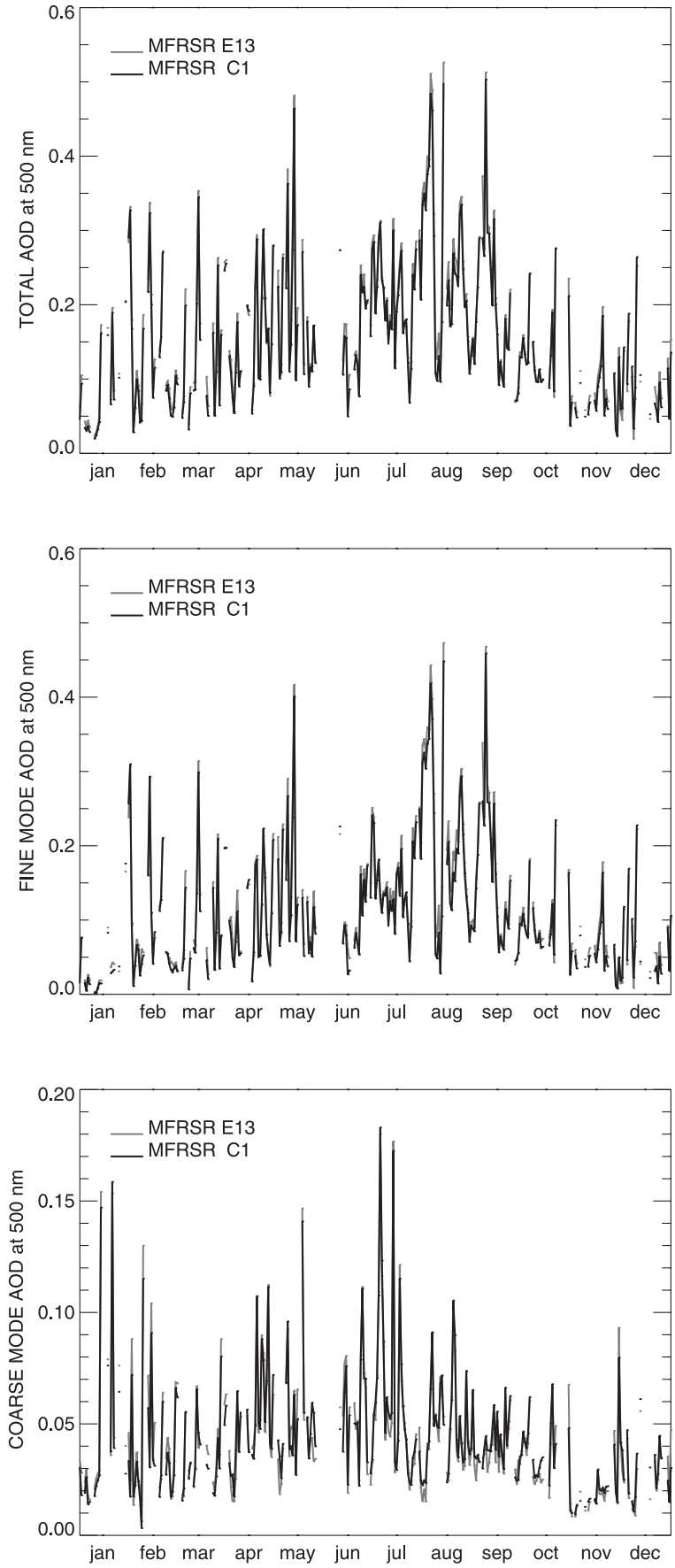
MFRSR E13
MFRSR C1
TOTAL AOD at 500 nm
0.0
0.2
0.4
0.6
jan feb mar apr may jun jul aug sep oct nov dec
MFRSR E13
MFRSR C1
FINE MODE AOD at 500 nm
0.0
0.2
0.4
0.6
jan feb mar apr may jun jul aug sep oct nov dec
MFRSR E13
MFRSR C1
COARSE MODE AOD at 500 nm
0.00
0.05
0.10
0.15
0.20
jan feb mar apr may jun jul aug sep oct nov dec

Figure 7

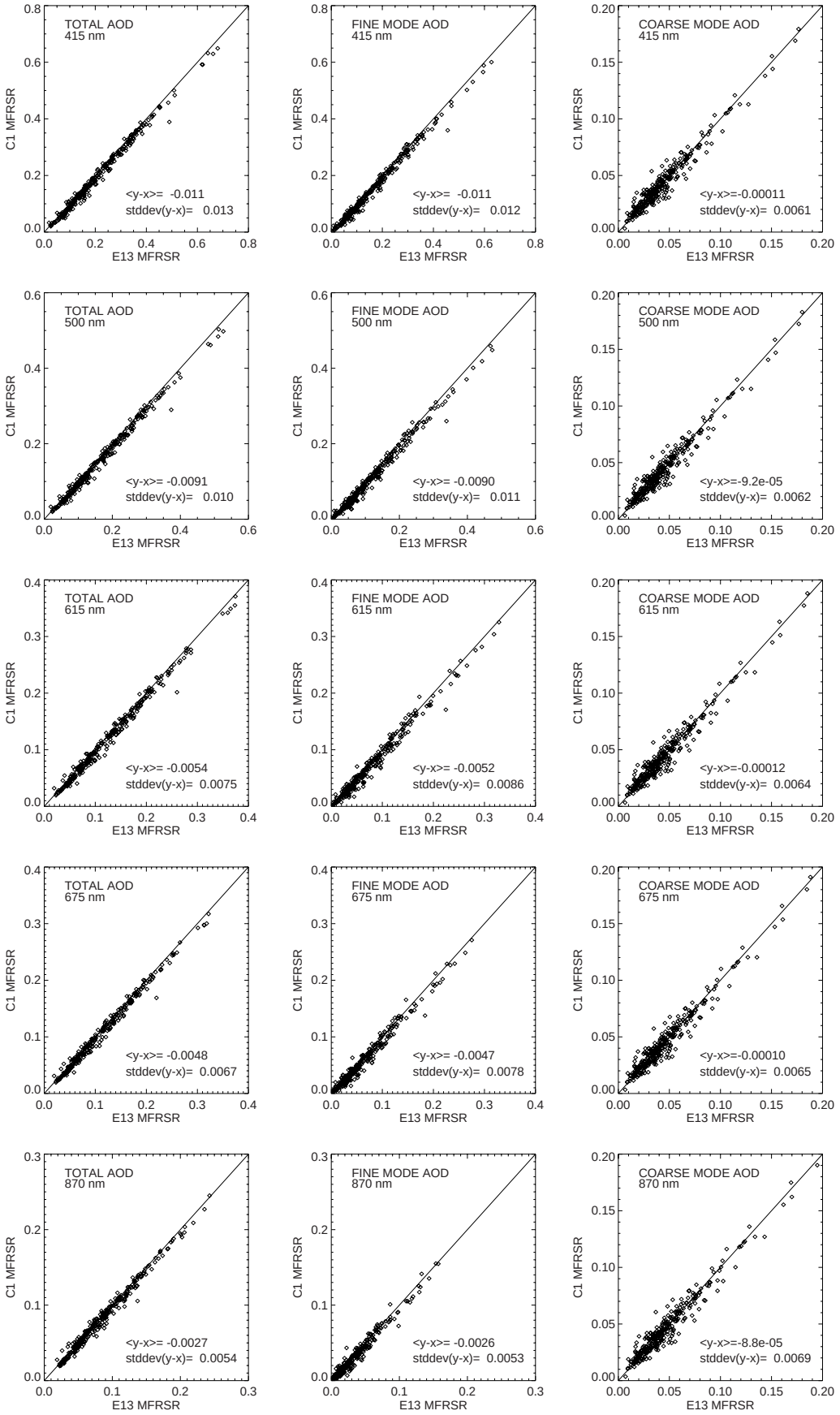

Figure 8. Intercomparison between daily mean total, fine, and coarse mode AODs retrieved from two MFRSRs (C1 and E13) data for the year 2000.

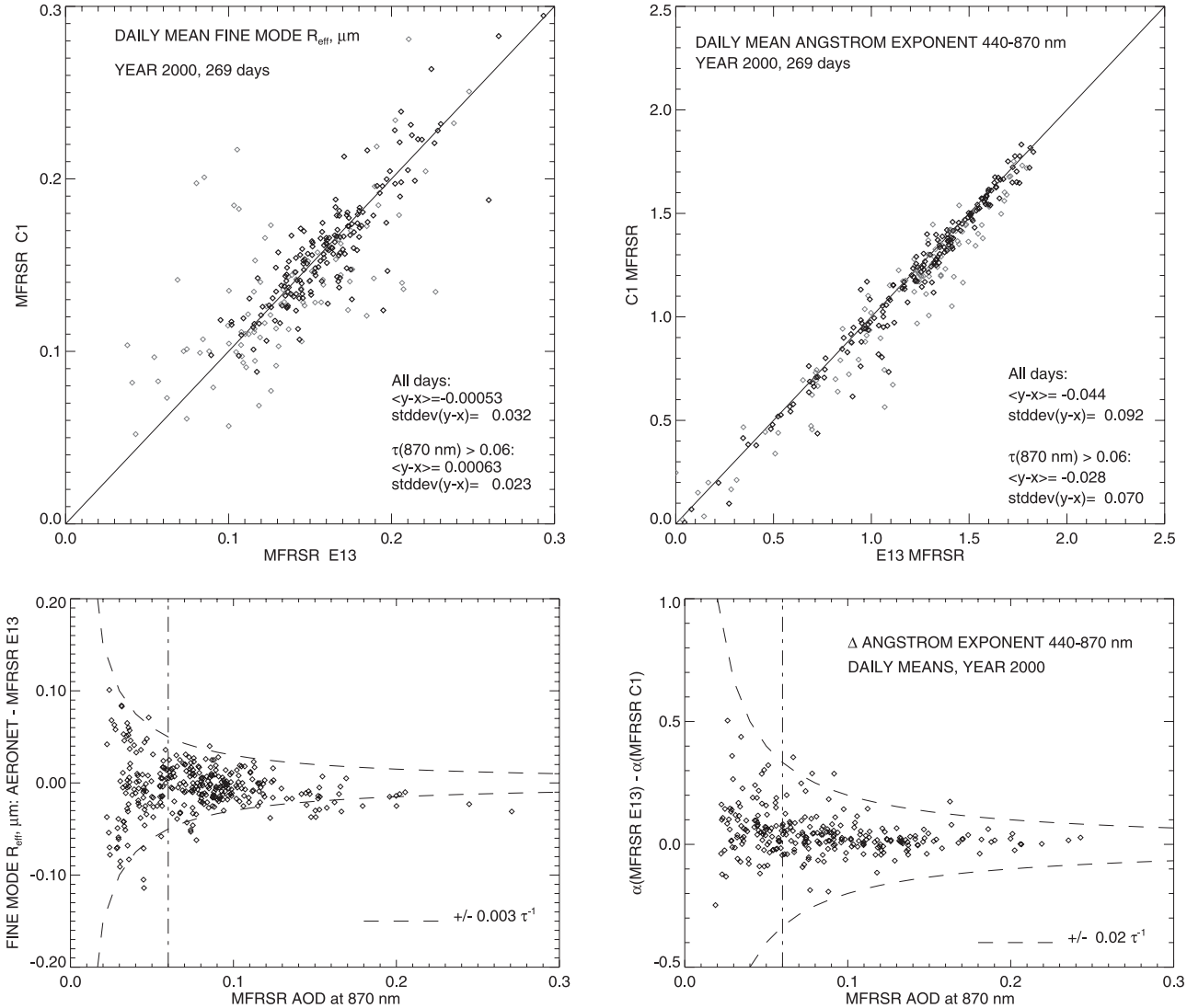

Figure 9. (top) Intercomparison between daily mean (left) fine mode r_{eff} and (right) 440–870 nm Angstrom exponent retrievals from C1 and E13 MFRSRs. (bottom) Dependencies of the differences between the two MFRSRs on 870 nm (MFRSR) AOD magnitude. The dashed curves depict the scaled inverse AODs, while our recommended threshold AOD value of 0.06 is shown by vertical dash-dotted lines.

to constrain the aerosol coarse mode and to derive single scattering albedo (SSA). In this intercomparison we used the recently released Version 2 AERONET retrievals for the year 2000. These retrievals are made with climatological amounts of NO_2 (similar to those used in our algorithm) and ozone. Unlike the MFRSRs intercomparisons described above (in which we used daily means) the MFRSR-AERONET scatterplots in this paper show point-by-point comparisons, where the MFRSR retrievals are taken from the data point which is closest to a CIMEL almucantar measurement and is located within 5 min from it. We use daily mean values, however, to compare the data sets as time series.

[35] While MFRSR and CIMEL Sun photometers have different spectral channel sets, we compared our retrievals of total, fine, and coarse mode AOD for three CIMEL wavelengths: 870 and 670 nm, that are common for both instruments, and 440 nm for which MFRSR AODs were linearly interpolated from the 415 and 500 nm channels. The results of point-by-point comparison between C1 MFRSR and AERONET are shown in Figure 11 (comparison between AERONET and E13 MFRSR looks similar, thus, we omit the corresponding plot). The plot includes 301 data points from 92 clear and partially clear days. We see small (about 0.01) overestimation of total AOD by MFRSR compared to CIMEL in all three channels. This bias (common for both MFRSRs) is of the order of magnitude of the best measurement accuracy of both instruments. It is probably due mostly to difference in calibration procedures (CIMEL is calibrated by comparison with the master instrument at NASA Goddard Space Flight Center, while we derive MFRSR calibrations from the data). However, differences in wavelength between the instruments, and minor technical problems (e.g., MFRSR's tilt) may also

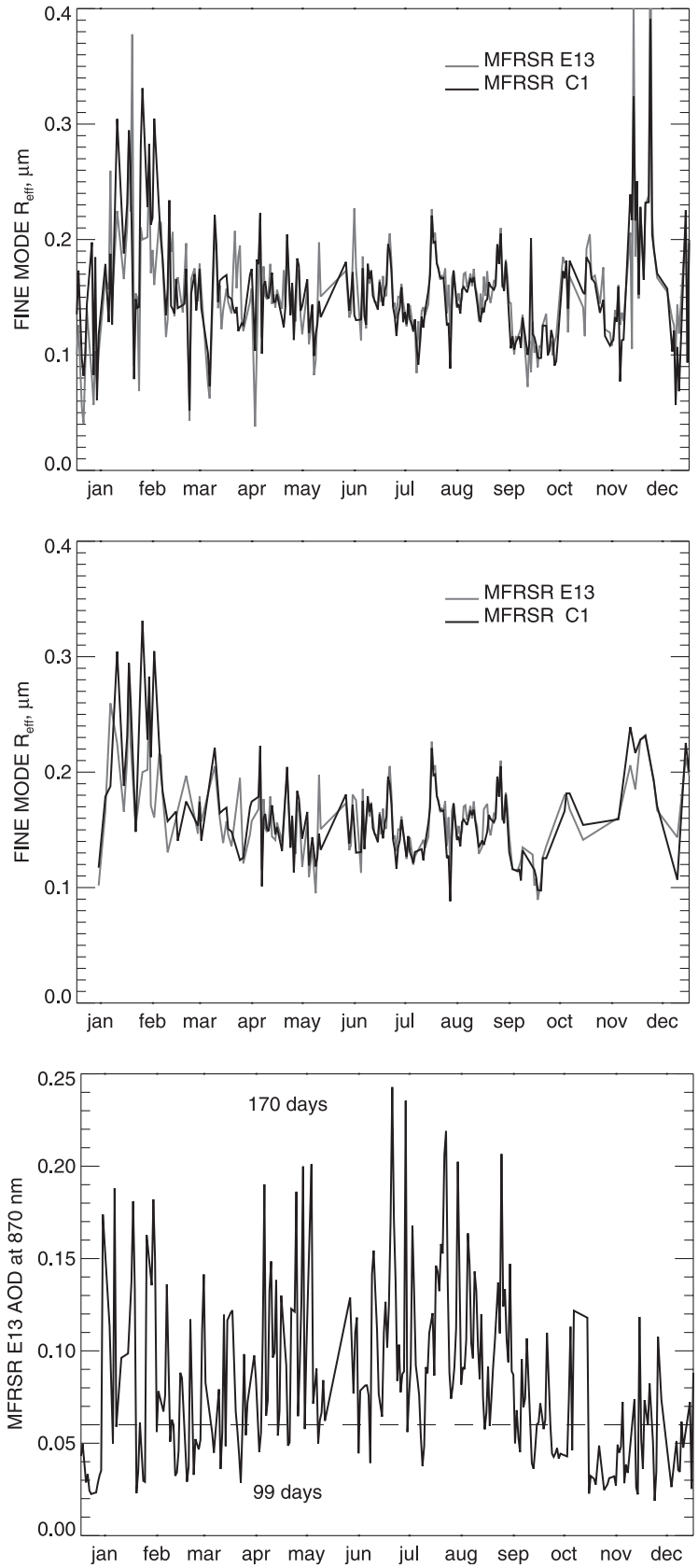

Figure 10. Intercomparison between time series of daily mean fine mode r_{eff} values from C1 and E13 MFRSRs. (top) All days from year 2000 with available retrievals, (middle) days with τ(870 nm) >0.06, and (bottom) time series of daily mean values of AOD in 870 nm channel with indication of number of values above and below 0.06 threshold.

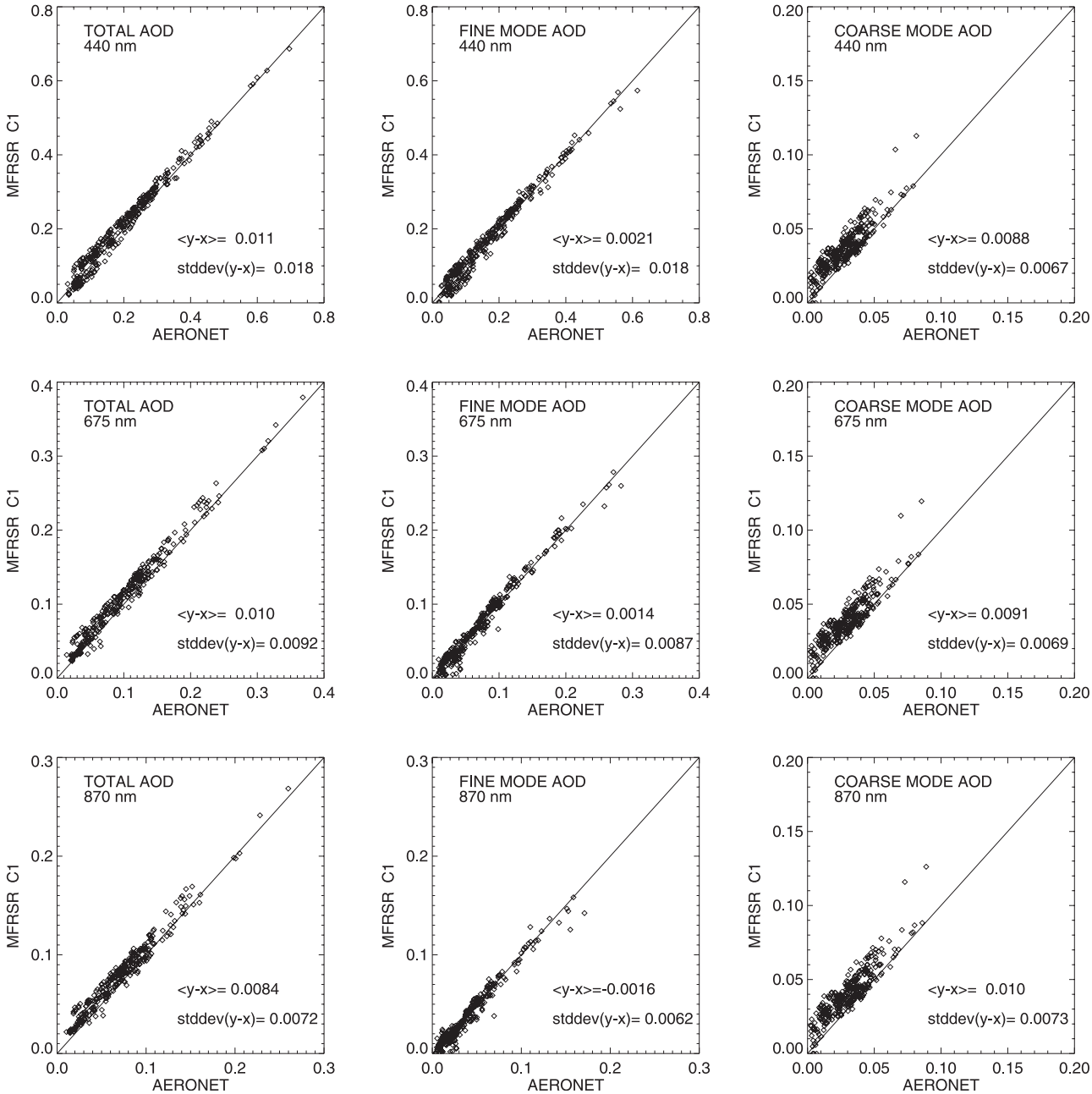

Figure 11. Point-by-point intercomparison between total, fine, and coarse mode AODs retrieved from MFRSR (C1) data and corresponding AERONET almucantar scan retrievals for the year 2000. The AERONET's CIMEL Sun photometer is colocated with MFRSR at SGP's Central Facility.

contribute to the disagreement. For C1 MFRSR this bias is translated mostly to coarse mode, while the fine mode AODs show even better agreement with AERONET than the total. As expected, the random error (standard deviation of the differences) in total AOD decreases with the wavelength from 0.018 at 440 nm to 0.007 at 870 nm. The random errors in coarse mode AOD are around 0.007 for all three wavelengths. The results for E13 MFRSR are only slightly different.

[36] Figure 12 shows comparison between time series of daily mean fine mode r_{eff} values from MFRSR and AERONET retrievals for the whole year. Data points with $\tau(870\ \mathrm{nm}) < 0.06$ are not removed from these plots to keep longer records. However, the observed agreement is still remarkable, especially in July–September (which has the highest density of AERONET's observations) and in January–March (in particular for E13). Figures 13 and 14 show point-by-point comparison between MFRSR and AERONET retrievals of respectively fine r_{eff} and 440–870 nm Angstrom exponent. These plots support the above discussed relationship between the retrieval accuracy of aerosol size parameters (Angstrom exponent, fine mode r_{eff}, or fine mode fraction in AOD) and AOD magnitude. For example, Figure 13 shows that while MFRSRs and AERONET retrievals of fine mode r_{eff} have practically no relative bias (0.002 μm bias for C1 and 0.005 μm bias for

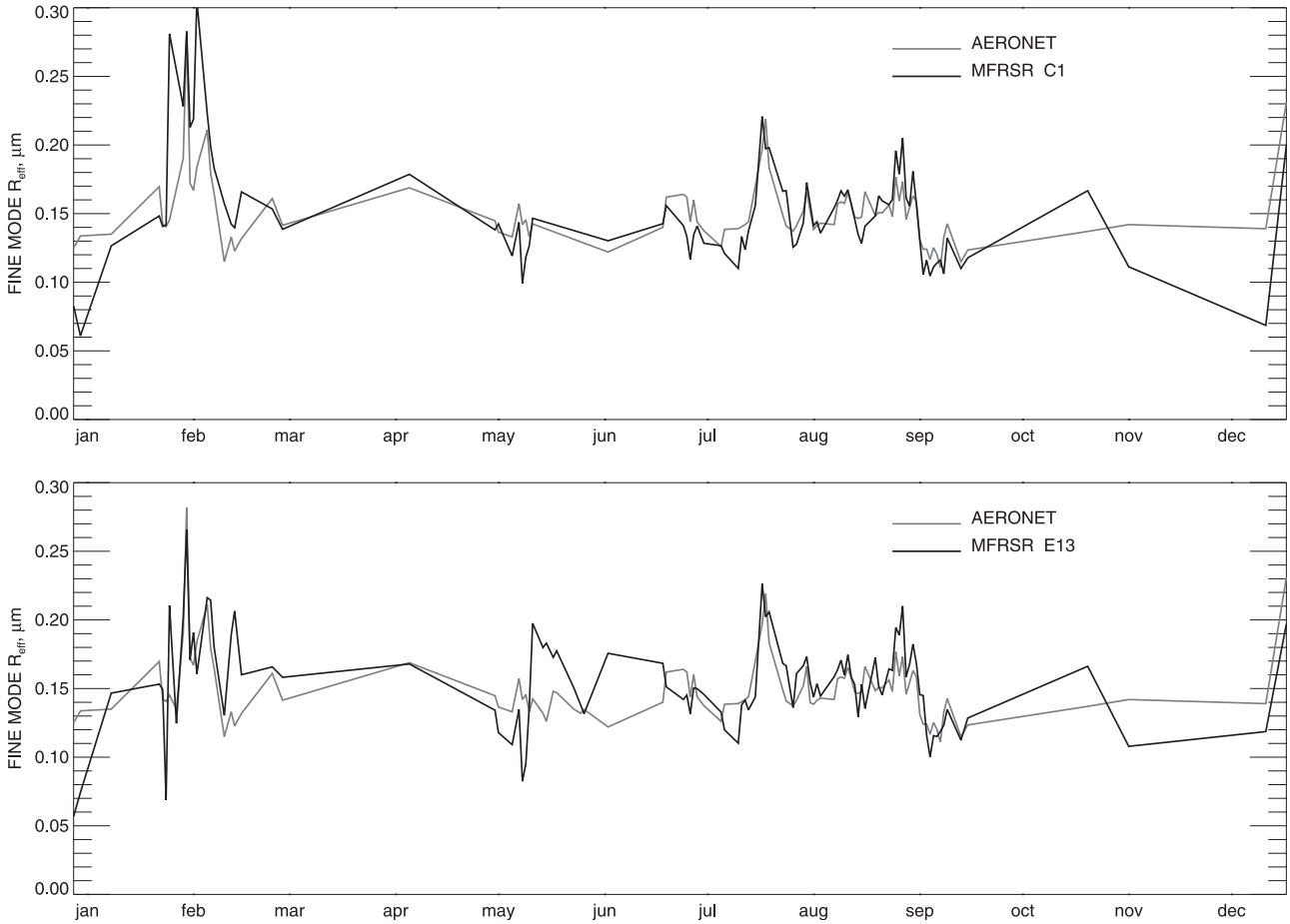

Figure 12. Comparison between time series of daily mean fine mode r_{eff} values from MFRSR ((top) C1 and (bottom) E13) and AERONET retrievals for the year 2000.

E13 relative to AERONET) the restriction τ(870 nm) >0.06 reduces the standard deviations of the differences by about a factor of two (from 0.036 to 0.016 μm for C1 and from 0.028 to 0.017 μm for E13). This reduced random error constitutes about 10% of a typical fine mode r_{eff} value (0.15 μm). Figure 13 (bottom) shows that the absolute MFRSR-AERONET differences in retrieved fine mode r_{eff} are bounded by the value (0.003 μm)/τ(870 nm) for almost all data points (the same bound as for two-MFRSR intercomparison in Figure 9 (bottom left)). From a similar comparison for 440–870 nm Angstrom exponents presented in Figure 14 we see that the largest differences between MFRSR and AERONET values are exhibited by a particular set of data points below one-one line (i.e., with AERONET values larger than those from MFRSRs), almost all of which correspond to τ(870 nm) < 0.06. Unlike in the fine mode r_{eff} case, this introduces a relative bias in retrievals in addition to a random error. This difference is not contradictory, since the Angstrom exponent in 440–870 nm spectral range depends on both fine and coarse mode AODs, and the bias seen in Figure 14 has passed into a corresponding bias in fine mode fraction ν_f (the plot is not shown because of lack of space). After the restriction on AOD magnitude is applied, these biases are significantly reduced (from −0.16 to −0.06 for C1 and from −0.09 to −0.01 for E13) together with the standard deviations reduced by a factor exceeding two (from 0.27 to 0.10 for C1 and from 0.23 to 0.10 for E13). As in the case of r_{eff}, the absolute differences between MFRSR and AERONET Angstrom exponent values are bounded by 0.02/τ(870) for almost all data points. The difficulties in AERONET retrievals related to characterization of aerosols under low optical depth conditions have been also reported by *Dubovik et al.* [2000]. They found that while the size distribution retrievals are sensitive to low AOD values, this problem more severely affects the retrievals of aerosol refractive index and single-scattering albedo. Thus, in most cases SSA retrievals are not recommended if τ(440 nm) is less than 0.5.

8. Further Analysis of Aerosol Size Parameters

[37] In this section we use the retrievals described above to more quantitatively asses the nature of various aerosol size parameters and relations between them. As mentioned in section 3, fine mode r_{eff} and fine mode fraction in 870 nm AOD (ν_f) may be physically correlated. This assertion is supported by Figure 15, which shows the MFRSR-derived daily mean values of these parameters as points in (ν_f, r_{eff}) plane (same plane as in Figure 4). Certain correlation between ν_f and r_{eff} can be seen in both top plots presenting respectively C1 and E13 data. Similar correlation is observed in AERONET data (Figure 16, top). This correlation

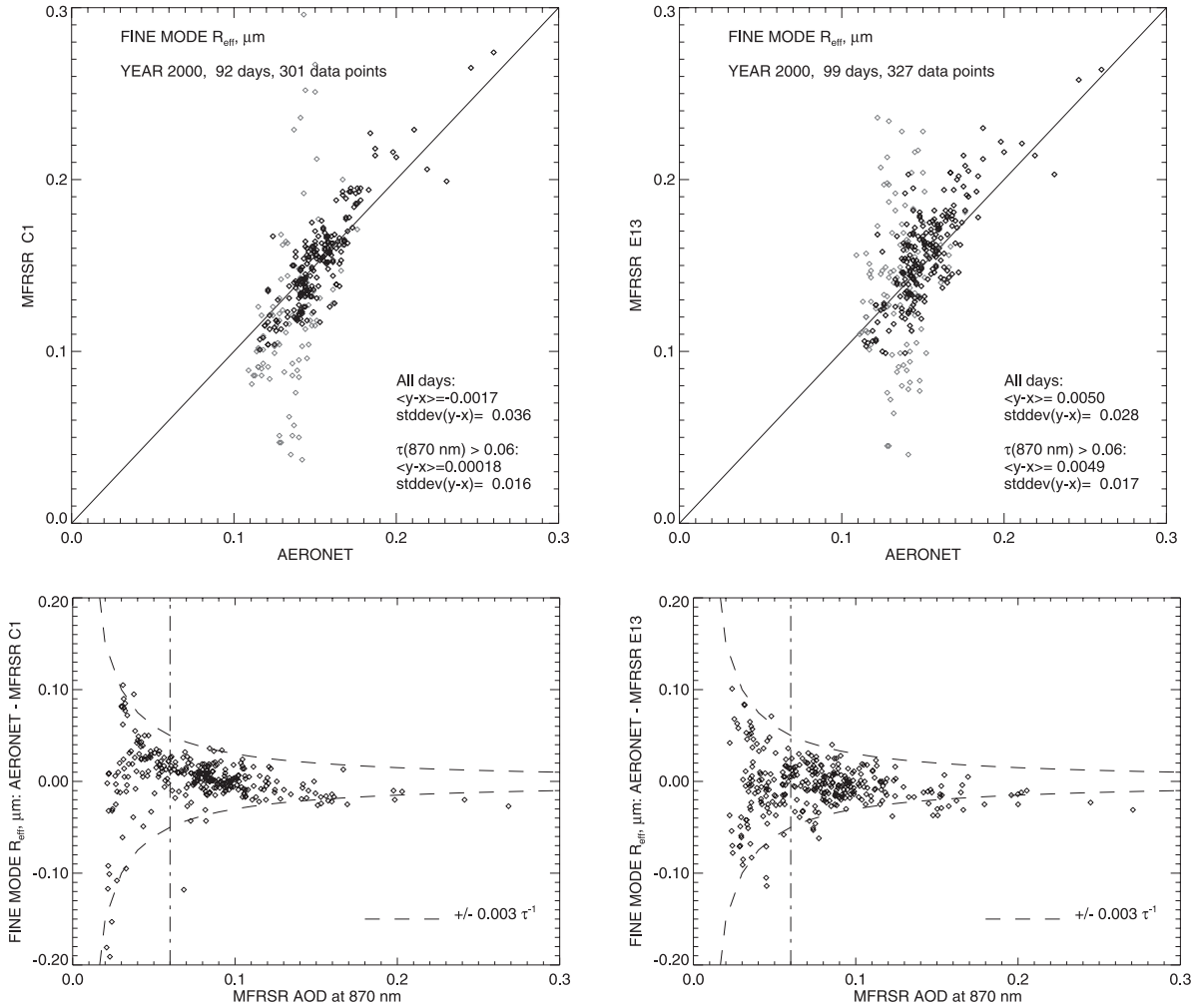

Figure 13. Point-by-point intercomparison between the fine mode effective radius values retrieved from MFRSR data ((left) C1 and (right) E13) and corresponding AERONET almucantar scan retrievals for the year 2000. (top) Scatterplots with black and grey diamonds representing the retrievals corresponding to τ(870 nm) larger and smaller than 0.06, respectively. (bottom) Dependence of the difference between MFRSR and AERONET values of r_{eff} on 870 nm (MFRSR) AOD. The dashed curves correspond to $\pm 0.003/\tau$(870 nm), while our recommended threshold AOD value of 0.06 is shown by vertical dash-dotted lines.

reflects the dependence of aerosol extinction on particle size. Indeed, at fixed fine mode number fraction $\hat{\nu}_f$ (4) an increase in fine mode particle radius would lead to an increase of fine mode AOD, and, therefore, in ν_f. This observation is supported by the fact, that the plot of r_{eff} versus fine mode particle number fraction $\hat{\nu}_f$ for AERONET data set (Figure 16, bottom) has no pronounced slope; that is, fine mode particle size is not correlated with relative concentration of fine particles. The time series for $\hat{\nu}_f$ were computed according to (8) using the actual values of fine and coarse r_{eff}, while v_{eff} (not provided in AERONET data set) were assumed to be 0.2 for both modes. We note, that the latter assumption is not generally true: direct comparison with AERONET-derived size distributions showed wide variability of v_{eff} for both modes. The differences between Figure 15 (top) and Figure 15 (middle) are shown in Figure 15 (bottom) by lines connecting the corresponded C1 and E13 (ν_f, r_{eff}) points. Though messy, it still shows a resemblance to the level curves in Figure 4. It also indicates differences in solution stability between different parameter ranges: e.g., for small ν_f even small measurement error may significantly affect the retrieved fine particle size.

[38] Figure 17 compares variability of the observed 415–870 nm Angstrom exponent (Figure 17, top left) with those of the fine mode fraction in AOD (Figure 17, top right) and fine mode r_{eff} (Figure 10). Figure 17 (bottom) demonstrates that the Angstrom exponent variability (with summer maximum [cf. *Michalsky et al.*, 2001]) is caused largely by the variability of the fine mode fraction in AOD (91% correlation), rather than the fine mode r_{eff} (23% anticorrelation). *Schuster et al.* [2006] came to a similar conclusion based on a study of AERONET Sun-sky inversions.

9. Discussion of NO_2-Related Issues in Aerosol Retrievals

[39] It has been previously noted [*Shaw*, 1976; *Schroeder and Davies*, 1987; *Alexandrov et al.*, 2002a], that inversion

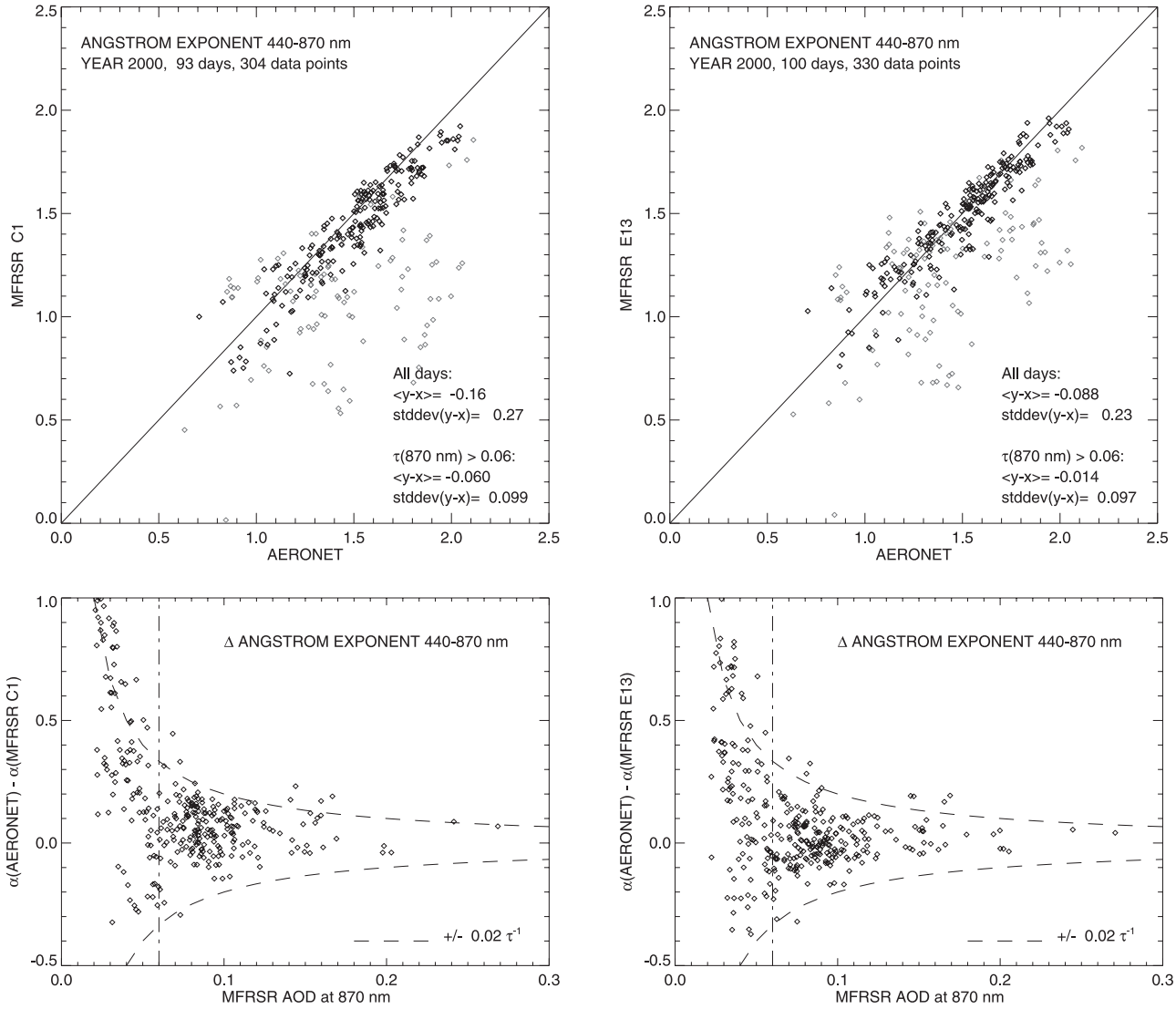

Figure 14. Same as in Figure 13 but for 440–870 nm Angstrom exponent.

of aerosol size from Sun photometric data is complicated by the trade-offs between spectral absorption of NO_2 in blue visible range and extinction of small aerosol particles. This problem is important for both MFRSR and AERONET CIMEL retrievals. There are two main ways to deal with the NO_2 issue. The first way is to constrain the NO_2 amount either by assuming a certain value (e.g., zero) or by taking it from an external source, such as satellite measurements, or climatology. The second way is to retrieve NO_2 amount from the data imposing certain conditions on aerosol size distribution and its variability in time, and then validate and possibly adjust the retrieval approach by comparison with external NO_2 measurements. AERONET's choice regarding treatment of NO_2 in aerosol retrievals was originally to neglect it, but in the recently released Version 2 retrieval product satellite-based NO_2 climatology is used. NO_2 was also neglected in MFRSR retrievals by *Kassianov et al.* [2005, 2007], while *Alexandrov et al.* [2002a, 2005] included NO_2 retrievals.

[40] Satellite retrievals of NO_2 columns from GOME [*Burrows et al.*, 1999; *Richter and Burrows*, 2002] and more recently SCIAMACHY [*Bovensmann et al.*, 1999; *Richter et al.*, 2004, 2005] have been available for several years, however these measurements have limited accuracy over populated areas where a significant fraction of the NO_2 is located in the boundary layer (below 1–3 km from the ground). The comprehensive sensitivity study by *Boersma et al.* [2004] concludes, that tropospheric NO_2 columns can be retrieved with a precision of 35–60% over regions with a large contribution of the tropospheric NO_2 to the total column. These retrieval uncertainties are dominated by the uncertainty in the estimate of the tropospheric air mass factor (AMF) influenced in its turn by the uncertainties in cloud fraction, surface albedo and a priori NO_2 profile shape. The AMF corrects for the different sensitivity of the measurements to absorption in different altitudes, which, according to *Richter et al.* [2004], is of particular importance for absorbers located close to the surface. *Boersma et al.* [2004] also emphasize the need to account for the temperature dependence of the NO_2 cross section, since neglect of the effective NO_2 temperature leads to systematic

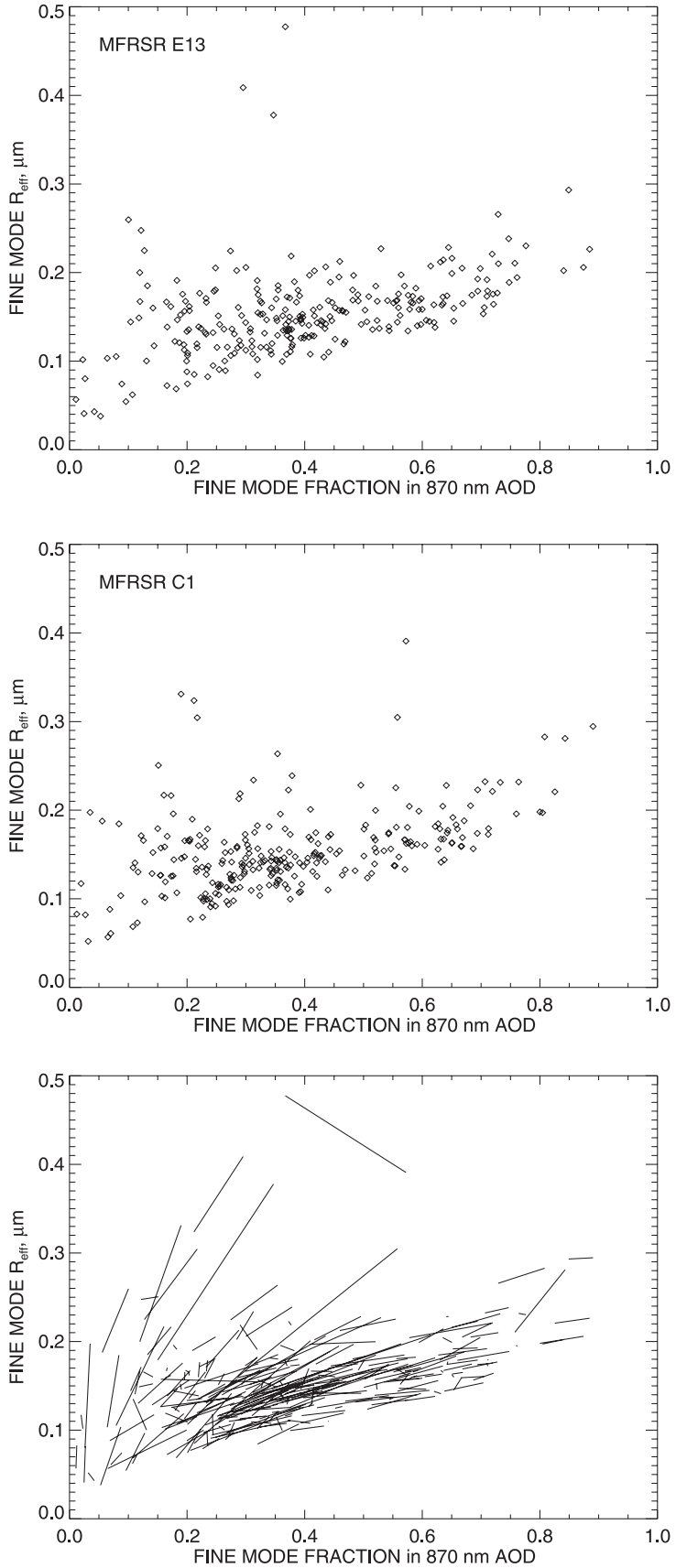

Figure 15. Daily mean values of fine mode r_{eff} versus the corresponding values of fine mode fraction in 870 nm AOD for (top) E13 and (middle) C1 MFRSRs. (bottom) Differences in the retrievals from Figure 15 (top and middle) depicted by lines connecting the corresponding (v_f, r_{eff}) points.

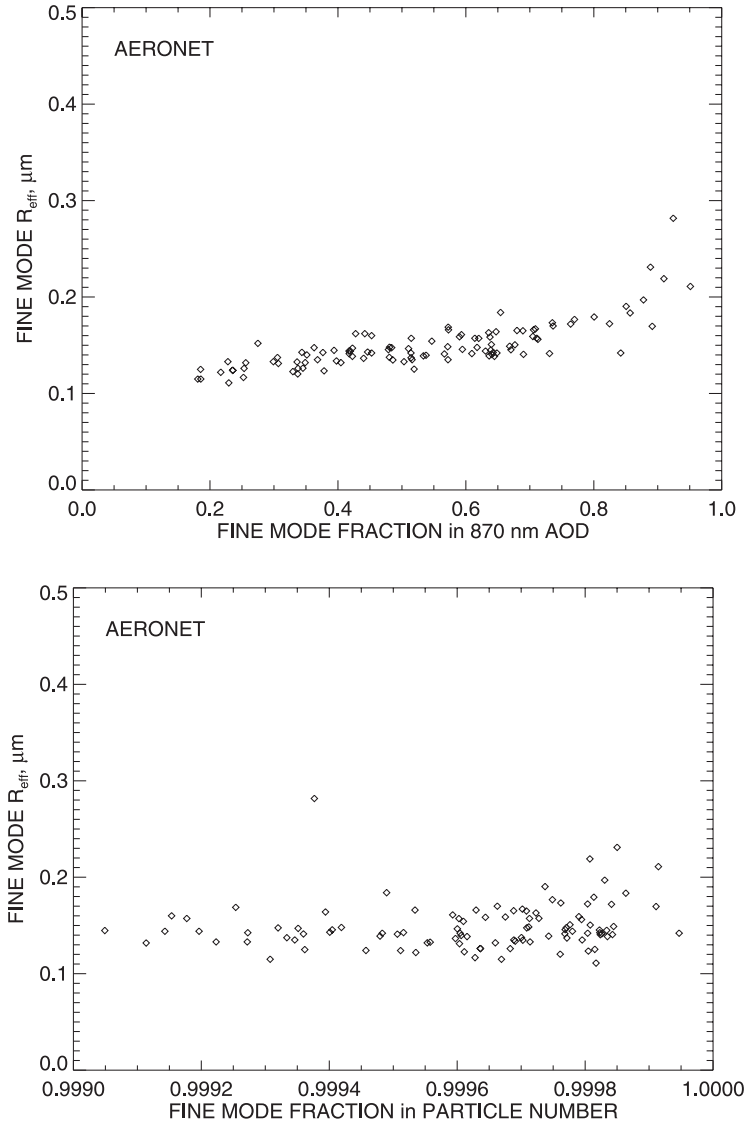

Figure 16. (top) Same as in Figure 15 (top) but for AERONET daily mean retrievals. (bottom) Same as Figure 16 (top) but with fine mode number fraction $\hat{v}_f$ (8) as x axis. Actual values of fine and coarse r_{eff} were used for computation of $\hat{v}_f$, while v_{eff} (not provided in AERONET data set) were assumed to be 0.2 for both modes.

underestimating of NO_2 columns in polluted areas by up to 20% because of warmer boundary layer NO_2.

[41] The uncertainties in satellite retrievals could be resolved by ground-based spectrometric studies especially in urban and industrial environments. However, until recently the available studies were primarily focused on stratospheric NO_2, or, in few cases, on the extreme NO_2 pollution events [e.g., *Schroeder and Davies*, 1987; *Pujadas et al.*, 2000; *Kambezidis et al.*, 2001], reporting up to 12 DU column at a suburban site in Canada and even 150 DU during a photochemical smog event in Athens, Greece. These two kinds of studies show essentially the wings of the statistical distribution of NO_2 column, providing little information on the typical values. Recently the situation was improved with publication of several spectrometric studies mostly devoted to validation of GOME and SCIAMACHY measurements [*Petritoli et al.*, 2004; *Heue et al.*, 2005; *Wang et al.*, 2005; *Gianelli et al.*, 2005; *Cede et al.*, 2006] over areas moderately affected by urban or industrial pollutions. For example, the measurements by airborne AMAXDOAS spectrometer in Germany reported by *Wang et al.* [2005] show vertical columns of up to 5.7×10^{16} molec cm^2 (2.1 DU, 1 DU = 2.687×10^{16} molec cm^2) observed close to Frankfurt, with a vertical distribution peaking in the boundary layer. A similar study by *Heue et al.* [2005] shows tropospheric vertical column over the polluted Po valley in Italy varying between 1.62 and 3.52×10^{16} molec cm^2 (0.6–1.3 DU) while the correlative SCIAMACHY data resulted in 1.99 to 3.70×10^{16} molec cm^2 (0.74–1.38 DU). The values retrieved by *Gianelli et al.* [2005] from the rotating shadowband spectroradiometer (RSS) located in a rural northern Oklahoma site (SGP's Central Facility) range from 0.05 to 0.8 DU with the mean of 0.3 DU. NO_2 column amounts measured by Brewer

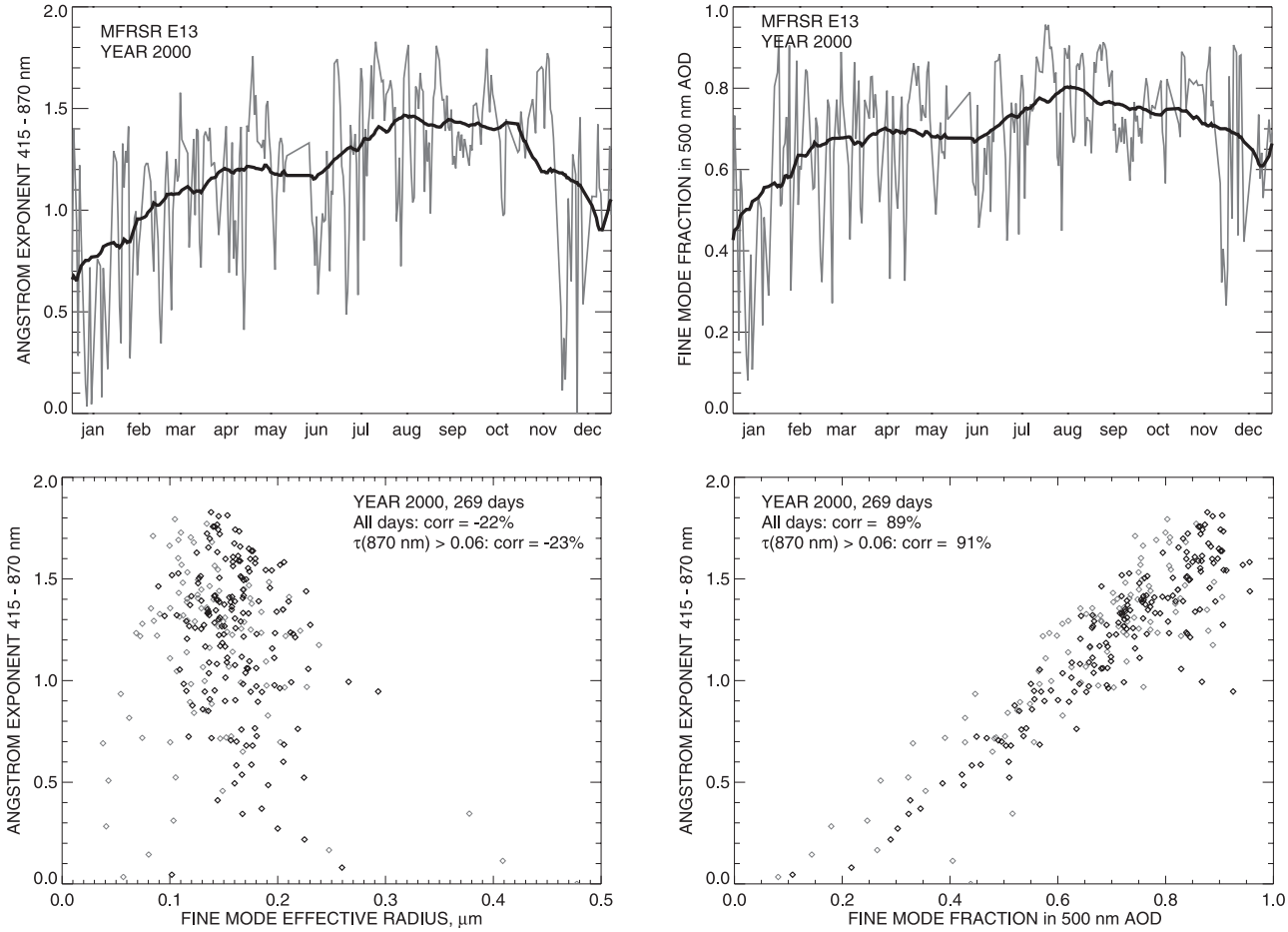

Figure 17. Interpretation of the (top left) 415–870 nm Angstrom exponent variability in terms of variabilities of fine mode r_{eff} (Figure 10) and (top right) fine mode fraction in 500 nm AOD. (bottom left and bottom right) The respective correlation plots. Black and grey diamonds represent the retrievals corresponding to τ(870 nm) larger and smaller than 0.06, respectively.

spectrometer at NASA Goddard Space Flight Center, Greenbelt, Maryland (suburban location) range form 0 to 3 DU with a mean of 0.7 DU [*Cede et al.*, 2006]. These measurements validate the satellite retrievals and provide realistic variability range of NO_2 column.

[42] Retrieval of NO_2 column from MFRSR or CIMEL measurements is possible in principle, but only if there is enough external information to significantly constrain the class of admissible aerosol size distributions. While using one nominal size distribution form may produce plausible results, another form could lead to incorrect NO_2 amounts. *Hansen and Travis* [1974] demonstrated that the angular dependence of aerosol phase function is constrained essentially by the effective radius and variance of the aerosol size distribution. However, a similar assertion about spectral dependence of AOD appears not to be true. In particular, there are strong spectral differences between AOD corresponding to monomodal and bimodal size distributions. Monomodal AOD tends to have a convex spectral shape with a maximum at a wavelength near the mode's effective radius, while bimodal AOD may be concave or decrease with the wavelength. Thus, AOD of a bimodal aerosol cannot be fitted well over the whole spectral range using a monomodal aerosol model. This means that if spectral AOD is fitted well in the aerosol-only 870 nm channel, the AOD values at short wavelengths, especially 415 nm, will be underestimated, and the difference can be interpreted as an excessive absorption optical depth of NO_2 (Figure 5), often significant.

[43] In our initial approach [*Alexandrov et al.*, 2002a] we adopted a family of simple monomodal size distributions parameterized by the effective radius r_{eff} and variance v_{eff}. These two parameters together with AOD (at, e.g., 870 nm) and NO_2 and ozone column amounts constitute 5 parameters to be derived from the ODs in the first 5 MFRSR channels. However, even with this inadequate aerosol model, it was evident, that the inversion problem was ill posed: there was a notable correlation between the retrieved r_{eff} and v_{eff} time series. This prompted *Alexandrov et al.* [2002a] to abandon retrieving v_{eff}, while provide the results for a number of fixed effective variances. This, however, did not correct the errors associated with using a monomodal aerosol model. The NO_2 column time series retrieved from the rural SGP's Central Facility data had strong correlation with AOD (with summer maximum) and reached values up to 15 DU, while the differential absorption measurements at

this site [*Gianelli et al.*, 2005] show an order of magnitude smaller values (0.8 DU at maximum). In our next study [*Alexandrov et al.*, 2005] a more realistic bimodal aerosol model was adopted. This model was essentially the same as that used in the present paper with the only difference: fine mode r_{eff} was not allowed to be smaller than 0.2 μm. This constraint was imposed to prevent the especially strong trade-offs between NO_2 and fine mode r_{eff} at small particle sizes. However, since the cutoff value for r_{eff} was too large, the values of NO_2 retrieved with that aerosol model were still too high (smaller by only about a factor of two compared with [*Alexandrov et al.*, 2002b]), and well correlated with AOD.

[44] The optical depth of 1 DU of NO_2 in 415, 500, and 615 nm MFRSR channels is 0.016, 0.006, and 0.001; it is practically zero at 670 and 870 nm. This means that optical depth corresponding to typical NO_2 column values described above is on the margins of the OD measurement accuracy (±0.01). We also demonstrated that given a wide enough class of realistic aerosol size distributions the ambiguity of fitting the data by "aerosol + NO_2" models is so large, that it essentially makes NO_2 nonretrievable from Sun photometric data. These considerations prompted us to adopt a new approach presented in this paper, which uses external NO_2 and ozone measurements.

10. Conclusions

[45] We describe recent improvements in our retrieval of aerosol parameters from MFRSR data, the main difference being the use of external measurements of NO_2 and ozone column amounts instead of simultaneous retrievals from the data [*Alexandrov et al.*, 2002a, 2005]. Sensitivity of aerosol size retrievals to measurement uncertainties and model assumptions was thoroughly examined, with particular emphasis on the role of NO_2. We also discuss available NO_2 measurements and the ways absorption by this gas was treated in previous aerosol studies.

[46] The consistency of our retrievals of total, fine, and coarse mode AOD, and fine mode aerosol effective radius is demonstrated by intercomparison between two collocated MFRSRs. The MFRSR retrievals were also validated by comparison with AERONET's Sun-sky inversion results. The measurements used for this intercomparison were made during the year 2000 by the two MFRSRs (C1 and E13) and AERONET CIMEL Sun photometer ("Cart-Site") located at the Central Facility of the Southern Great Plains (SGP) site run by the DOE Atmospheric Radiation Measurement (ARM) Program. The most recent (Version 2, Level 2) AERONET Sun-sky inversions were used.

[47] The intercomparison between the two MFRSRs showed very good agreement in retrievals of both AOD components and fine mode aerosol size. The magnitudes of relative biases in total AOD (Figure 8) were within the expected measurement accuracy (decreasing from 0.011 in 415 nm channel to 0.003 at 870 nm), while the random error (standard deviations of the differences) in AOD was between 0.013 at 415 nm and 0.005 at 870 nm, also decreasing with the channel wavelength. The relative biases in total AOD were translated primarily into corresponding biases in fine mode AOD, leaving the coarse mode AODs practically unbiased (with random error of 0.006–0.007). The estimates of the fine mode effective radius (Figure 9) from the two MFRSR data sets show practically no relative bias and agree within 0.03 μm random error. This random error decreases to 0.02 μm if only the data points with large enough AOD (τ(870 nm) >0.06) are selected. It appeared, that the absolute differences between the two instruments in retrievals of the parameters characterizing aerosol size, such as Angstrom exponent, fine mode r_{eff}, and fine mode fraction in AOD, are bounded from above by a value proportional to inverse AOD.

[48] The comparison of MFRSR-derived AODs with AERONET Sun-sky inversions used three wavelengths, two of which (675 and 870 nm) are common for MFRSR and CIMEL, and one (440 nm) is a CIMEL wavelength for which MFRSR AODs were linearly interpolated. This intercomparison showed that total, fine and coarse mode AOD retrievals from both MFRSRs agree well with AERONET data. For example, C1 MFRSR (Figure 11) shows only small (around 0.01) biases in total AOD compared to AERONET at all three selected wavelengths. These biases propagated mainly into the coarse mode AOD values. As expected, the random error in total AOD is larger (0.018) at 440 nm than at shorter wavelengths (0.009 and 0.007 respectively at 675 and 870 nm). The random errors in coarse mode AOD were of 0.007 and practically independent from wavelength. The agreement between the MFRSRs and AERONET in fine mode particle size estimates is impressive (Figure 12) especially for July–September data, when more AERONET measurements were available. Quantitatively this agreement is described (Figure 13) by the absence of bias in MFRSR-derived r_{eff} relative to AERONET values and small random error (0.036 μm for C1, 0.028 μm for E13), which is reduced by about a factor of two (0.016 μm for C1, 0.017 μm for E13) if the condition τ(870 nm) >0.06 is imposed. This error is about 10% of a typical fine mode r_{eff} value.

[49] In addition to retrieval intercomparison, we presented some further developments, showing relations between retrievals of fine mode r_{eff} and fine mode fractions in AOD and in particle number. We plan to extend validation of our retrieval algorithm to more measurement sites with different climatological conditions. An easy to use program package written in IDL language, able to automatically perform the retrievals from MFRSR data discussed in this article, is available from the authors.

[50] **Acknowledgments.** This research was supported by the Office of Biological and Environmental Research of the U.S. Department of Energy as part of the Atmospheric Radiation Measurement Program. We would like to thank A. Richter for providing overpass NO_2 SCIAMACHY data for SGP and R. Wagener for his effort to maintain AERONET site at SGP's Central Facility.

References

Ackerman, T. P., and G. Stokes (2003), The Atmospheric Radiation Measurement Program, *Phys. Today*, *56*, 38–45.

Alexandrov, M., A. Lacis, B. Carlson, and B. Cairns (2002a), Remote sensing of atmospheric aerosols and trace gases by means of Multi-Filter Rotating Shadow-band Radiometer. Part I: Retrieval algorithm, *J. Atmos. Sci.*, *59*, 524–543.

Alexandrov, M., A. Lacis, B. Carlson, and B. Cairns (2002b), Remote sensing of atmospheric aerosols and trace gases by means of Multi-Filter Rotating Shadow-band Radiometer. Part II: Climatological applications, *J. Atmos. Sci.*, *59*, 544–566.

Alexandrov, M. D., A. Marshak, B. Cairns, A. A. Lacis, and B. E. Carlson (2004), Automated cloud screening algorithm for MFRSR data, *Geophys. Res. Lett.*, *31*, L04118, doi:10.1029/2003GL019105.

Alexandrov, M. D., B. E. Carlson, A. A. Lacis, and B. Cairns (2005), Separation of fine and coarse aerosol modes in MFRSR data sets, *J. Geophys. Res.*, *110*, D13204, doi:10.1029/2004JD005226.

Alexandrov, M. D., P. Kiedron, J. J. Michalsky, G. Hodges, C. J. Flynn, and A. A. Lacis (2007), Optical depth measurements by shadow-band radiometers and their uncertainties, *Appl. Opt.*, *46*, 8027–8038.

Augustine, J. A., G. B. Hodges, C. R. Cornwall, J. J. Michalsky, and C. I. Medina (2005), An update on SURFRAD—The GCOS Surface Radiation budget network for the continental United States, *J. Atmos. Oceanic Technol.*, *22*, 1460–1472.

Bigelow, D. S., J. R. Slusser, A. F. Beaubien, and J. H. Gibson (1998), The USDA Ultraviolet Radiation Monitoring Program, *Bull. Am. Meteorol. Soc.*, *79*, 601–615.

Boersma, K. F., H. J. Eskes, and E. J. Brinksma (2004), Error analysis for tropospheric NO2 retrieval from space, *J. Geophys. Res.*, *109*, D04311, doi:10.1029/2003JD003962.

Bovensmann, H., J. P. Burrows, M. Buchwitz, J. Frerick, S. Noel, V. V. Rozanov, K. V. Chance, and A. H. P. Goede (1999), SCIAMACHY—Mission objectives and measurement modes, *J. Atmos. Sci.*, *56*, 127–150.

Burrows, J. P., et al. (1999), The Global Ozone Monitoring Experiment (GOME): Mission concept and first scientific results, *J. Atmos. Sci.*, *56*, 151–175.

Cede, A., J. Herman, A. Richter, N. Krotkov, and J. Burrows (2006), Measurements of nitrogen dioxide total column amounts using a Brewer double spectrometer in direct Sun mode, *J. Geophys. Res.*, *111*, D05304, doi:10.1029/2005JD006585.

Cleveland, W. S. (1979), Robust locally weighted regression and smoothing scatterplots, *J. Am. Stat. Assoc.*, *74*, 829–836.

Dubovik, O., and M. D. King (2000), A flexible inversion algorithm for retrieval of aerosol optical properties from Sun and sky radiance measurements, *J. Geophys. Res.*, *105*, 20,673–20,696.

Dubovik, O., A. Smirnov, B. N. Holben, M. D. King, Y. J. Kaufman, T. F. Eck, and I. Slutsker (2000), Accuracy assessments of aerosol optical properties retrieved from AERONET Sun and sky radiance measurements, *J. Geophys. Res.*, *105*, 9791–9806.

Dubovik, O., B. Holben, T. F. Eck, A. Smirnov, Y. J. Kaufman, M. D. King, D. Tanre, and I. Slutsker (2002), Variability of absorption and optical properties of key aerosol types observed in worldwide locations, *J. Atmos. Sci.*, *59*, 590–608.

Forgan, B. W. (1988), Sun photometer calibration by the ratio-Langley method, in *Baseline Atmospheric Program (Australia) 1986*, edited by B. W. Forgan and P. J. Fraser, pp. 22–26, Bur. of Meteorol., Melbourne, Vic., Australia.

Forgan, B. W. (1994), General method for calibrating Sun photometers, *Appl. Opt.*, *33*, 4841–4850.

Gianelli, S. M., B. E. Carlson, and A. A. Lacis (2005), Aerosol retrievals using rotating shadowband spectroradiometer data, *J. Geophys. Res.*, *110*, D05203, doi:10.1029/2004JD005329.

Hansen, J. E., and L. D. Travis (1974), Light scattering in planetary atmospheres, *Space Sci. Rev.*, *16*, 527–610.

Harrison, L., J. Michalsky, and J. Berndt (1994), Automated multifilter shadow-band radiometer: Instrument for optical depth and radiation measurement, *Appl. Opt.*, *33*, 5118–5125.

Harrison, L., P. Kiedron, J. Berndt, and J. Schlemmer (2003), Extraterrestrial solar spectrum 360–1050 nm from rotating shadowband spectroradiometer measurements at the Southern Great Plains (ARM) site, *J. Geophys. Res.*, *108*(D14), 4424, doi:10.1029/2001JD001311.

Heue, K.-P., A. Richter, M. Bruns, J. P. Burrows, C. von Friedeburg, U. Platt, I. Pundt, P. Wang, and T. Wagner (2005), Validation of SCIAMACHY tropospheric NO_2-columns with AMAXDOAS measurements, *Atmos. Chem. Phys.*, *5*, 1039–1051.

Holben, B. N., et al. (1998), AERONET—A federated instrument network and data archive for aerosol characterization, *Remote Sens. Environ.*, *66*, 1–16.

Kambezidis, H. D., A. D. Adamopoulos, and C. Gueymard (2001), Total NO_2 column amount over Athens, Greece in 1996–97, *Atmos. Res.*, *57*, 1–8.

Kassianov, E. I., J. C. Barnard, and T. P. Ackerman (2005), Retrieval of aerosol microphysical properties using surface multifilter rotating shadowband radiometer (MFRSR) data: Modeling and observations, *J. Geophys. Res.*, *110*, D09201, doi:10.1029/2004JD005337.

Kassianov, E. I., C. J. Flynn, T. P. Ackerman, and J. C. Barnard (2007), Aerosol single-scattering albedo and asymmetry parameter from MFRSR observations during the ARM Aerosol IOP 2003, *Atmos. Chem. Phys.*, *7*, 3341–3351.

Kiedron, P. W., J. J. Michalsky, J. L. Berndt, and L. C. Harrison (1999), Comparison of spectral irradiance standards used to calibrate shortwave radiometers and spectroradiometers, *Appl. Opt.*, *38*, 2432–2439.

Michalsky, J. J., J. C. Liljegren, and L. C. Harrison (1995), A comparison of sunphotometer derivations of total column water vapor and ozone to standard measures of same at the Southern Great Plains Atmospheric Radiation Measurement site, *J. Geophys. Res.*, *100*, 25,995–26,003.

Michalsky, J. J., J. A. Schlemmer, W. E. Berkheiser, J. L. Berndt, L. C. Harrison, N. S. Laulainen, N. R. Larson, and J. C. Barnard (2001), Multiyear measurements of aerosol optical depth in the Atmospheric Radiation Measurement and Quantitative Links programs, *J. Geophys. Res.*, *106*, 12,099–12,107.

Mitchell, R. M., and B. W. Forgan (2003), Aerosol measurement in the Australian Outback: Intercomparison of Sun photometers, *J. Atmos. Oceanic Technol.*, *20*, 54–66.

Ohmura, A., et al. (1998), Baseline Surface Radiation Network (BSRN/WCRP): New precision radiometry for Climate research, *Bull. Am. Meteorol. Soc.*, *79*, 2115–2136.

Petritoli, A., P. Bonasoni, G. Giovanelli, F. Ravegnani, I. Kostadinov, D. Bortoli, A. Weiss, D. Schaub, A. Richter, and F. Fortezza (2004), First comparison between ground-based and satellite-borne measurements of tropospheric nitrogen dioxide in the Po basin, *J. Geophys. Res.*, *109*, D15307, doi:10.1029/2004JD004547.

Pujadas, M., J. Plaza, J. Terés, B. Artiñano, and M. Millán (2000), Passive remote sensing of nitrogen dioxide as a tool for tracking air pollution in urban areas: The Madrid urban plume, a case of study, *Atmos. Eviron.*, *34*, 3041–3056.

Richter, A., and J. P. Burrows (2002), Retrieval of tropospheric NO_2 from GOME measurements, *Adv. Space Res.*, *29*, 1673–1683.

Richter, A., V. Eyring, J. P. Burrows, H. Bovensmann, A. Lauer, B. Sierk, and P. J. Crutzen (2004), Satellite measurements of NO_2 from international Shipping emissions, *Geophys. Res. Lett.*, *31*, L23110, doi:10.1029/2004GL020822.

Richter, A., J. P. Burrows, H. Nüß, C. Granier, and U. Niemeier (2005), Increase in tropospheric nitrogen dioxide over China observed from space, *Nature*, *437*, 129–132, doi:10.1038/nature04092.

Schmid, B., P. R. Spyak, S. F. Biggar, C. Wehrli, J. Sekler, T. Ingold, C. Matzler, and N. Kampfer (1998), Evaluation of the applicability of solar and lamp radiometric calibrations of a precision Sun photometer operating between 300 and 1025 nm, *Appl. Opt.*, *37*, 3923–3941.

Schroeder, R., and J. A. Davies (1987), Significance of nitrogen dioxide absorption in estimating aerosol optical depth and size distributions, *Atmos. Ocean*, *25*, 107–114.

Schuster, G. L., O. Dubovik, and B. N. Holben (2006), Angstrom exponent and bimodal aerosol size distributions, *J. Geophys. Res.*, *111*, D07207, doi:10.1029/2005JD006328.

Shaw, G. E. (1976), Nitrogen dioxide–optical absorption in visible, *J. Geophys. Res.*, *81*, 5791–5792.

Taha, G., and G. P. Box (1999), New method for inferring total ozone and aerosol optical thickness from multispectral extinction measurements using eigenvalue analysis, *Geophys. Res. Lett.*, *26*, 3085–3088.

Wang, P., A. Richter, M. Bruns, V. V. Rozanov, J. P. Burrows, K.-P. Heue, I. Pundt, T. Wagner, and U. Platt (2005), Measurements of tropospheric NO_2 with an airborne multi axis DOAS instrument, *Atmos. Chem. Phys.*, *5*, 337–343.

M. D. Alexandrov, B. Cairns, B. E. Carlson, and A. A. Lacis, NASA Goddard Institute for Space Studies, 2880 Broadway, New York, NY 10027, USA. (malexandrov@giss.nasa.gov)